MOISTURE SENSITIVITY OF PLA/PBS BLENDS DURING ULTRASONIC WELDING AND FUSED DEPOSITION MODELING

A Thesis
Submitted to the Graduate Faculty
of the
North Dakota State University
of Agriculture and Applied Science

By

Raihan Quader

In Partial Fulfillment of the Requirements
for the Degree of
MASTER OF SCIENCE

Major Department:
Industrial and Manufacturing Engineering

October 2021

Fargo, North Dakota

North Dakota State University
Graduate School

Title

MOISTURE SENSITIVITY OF PLA/PBS BLENDS DURING ULTRASONIC WELDING AND FUSED DEPOSITION MODELING

By

Raihan Quader

The Supervisory Committee certifies that this ***disquisition*** complies with North Dakota State University's regulations and meets the accepted standards for the degree of

MASTER OF SCIENCE

SUPERVISORY COMMITTEE:

Dr. Lokesh Karthik Narayanan
Chair

Dr. David Grewell

Dr. Chad Ulven

Dr. Nita Yodo

Approved:

11/18/2021 — Date

Dr. David Grewell — Department Chair

ABSTRACT

Moisture absorption into hygroscopic/hydrophilic materials used in fused deposition modeling (FDM) and ultrasonic welding (USW) can diminish desired mechanical properties. Sensitivity to moisture is dependent on material properties and environmental factors and needs characterization. In this thesis, moisture sensitivity of PLA filaments and PLA/PBS blended filaments was characterized in FDM printed ASTM test samples post-conditioning the filaments at different relative humidity levels. Tensile strength decreased with increase in moisture content. Parts made with PLA 4043D, PLA/PBS 75/25 filaments were most sensitive to moisture. Investigation of tensile properties of parts made with PLA filaments exposed to room temperature and humidity conditions for three months showed a more significant decrease. Moisture sensitivity of PLA, PBS, and PLA/PBS 25/75 blend characterized for USW using injection-molded industrial standard test parts (ISTeP) showed a downward trend in weld strength for 100% PLA and PLA/PBS 25/75 while 100% PBS was significantly affected at high moisture conditions.

ACKNOWLEDGMENTS

At first, I praise and thank God for keeping me in excellent health and giving me such a great opportunity for pursuing my graduate studies.

I express my sincerest gratitude to my thesis advisor Dr. Lokesh Karthik Narayanan and IME department chair Dr. David Grewell for their continuous support and guidance.

In addition, I thank all the other committee members and department faculty and staff for their phenomenal teaching, research, and administrative services.

I would also like to thank the Center for Bioplastics and Biocomposites for funding this research.

Lastly, thanks to my family members and well-wishers for their prayers and help.

DEDICATION

This thesis is dedicated to my parents

Mr. Abdul Quader and Mrs. Farida Begum

TABLE OF CONTENTS

LIST OF TABLES

LIST OF FIGURES

LIST OF ABBREVIATIONS

AM .....Additive Manufacturing

FDM .....Fused Deposition Modeling

SLS .....Selective Laser Sintering

EBM .....Electron Beam Melting

3DP .....3-Dimensional Printing

SLA .....Stereolithography

CAD .....Computer-aided Design

STL .....Standard Tessellation Language

USB .....Universal Serial Bus

USW .....Ultrasonic Welding

ABS .....Acrylonitrile Butadiene Styrene

PLA .....Polylactic Acid

PBS .....Polybutylene Succinate

ISTeP .....Industrial Standard Test Part

DSC .....Differential Scanning Calorimetry

RH .....Relative Humidity

SEM .....Scanning Electron Microscope

MFI .....Melt Flow Index

ANOVA .....Analysis of Variance

1. INTRODUCTION

1.1. Fused Deposition Modeling

According to joint ISO/ASTM standard, AM is defined to be “the process of joining materials to make parts from 3D model data, usually layer upon layer, as opposed to subtractive manufacturing and formative manufacturing methodologies” [1]. AM processes can be classified into FDM, SLS, polyjet, EBM, 3DP, SLA and a few others based on the processed material type, working principle, and materials used [2].

FDM is the most widely used AM technique to date. S. Scott Crump first invented this technique in 1988 and patented his invention. A typical FDM printer operates based on the filament extrusion principle. The printer has a filament feeding system with drive wheels, a heater for melting the filament (referenced as liquefier in figure 1), a nozzle head, a build plate, and a frame to support all the parts [3]. FDM is a popular AM method for a variety of applications owing to the availability of relatively cheaper printers, materials, ease of control, and not requiring any post-processing or resin curing, [4].

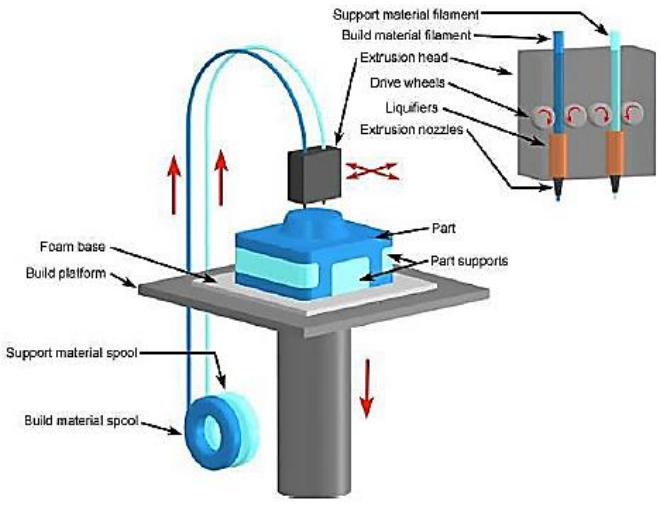

Figure 1. A general setup of an FDM 3D printer with various components [3]

The process flow of FDM starts with a CAD model of the part to be printed. The CAD file is then imported into slicing software for setting up the process parameters which vary according to the printer being used. After the process parameters are finalized, the file can either be exported as an STL file or be used directly from the software to print. The filament material has to be loaded in the extruder of the FDM printer before the printing can be started. Based on the complexity of the part, extra settings such as support structure, dual filament extruder, and other advanced settings might be needed.

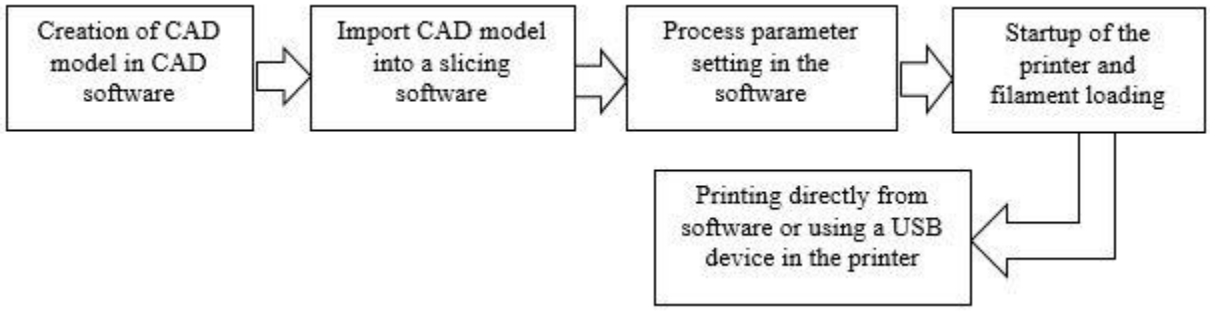

Figure 2. FDM process flow

Due to the unique advantages of FDM, it is being used in biomedical, aut omotive, architectural, and manufacturing of different commercial products. FDM is highly convenient in reducing the lead time to fabricate parts. It is a relatively accurate and less expensive process and satisfies the functional requirements of parts used in specific applications with lower mechanical workload requirements. Besides being very versatile, a variety of high-performance process-specific filament materials such as ULTEM™ 9085 (certified for use in the aerospace industry) are also adding value to the process thereby helping to achieve superior functional characteristics required in the intended product. In addition, there are various projects at different stages of research and development to develop advanced composite filaments and more robust printers to use these advanced filaments.

1.2. Ultrasonic Welding

Ultrasonic welding is a popular welding method used in thermoplastic and thermoplastic composite processing industry. In general, thermoplastic and thermoplastic composite welding is achieved by melting or softening the mating surfaces of the parts to be joined through the generation of heat through various techniques. Joint strength between two faying/welding surfaces is achieved through the intermolecular diffusion of polymer chains at the weld interface. There are different welding techniques available that can be classified according to the heating method used to melt the material. Two major categories are external and internal heating. Internal heating can again be subdivided into mechanical and electromagnetic internal heating. Ultrasonic welding is a form of mechanical internal heating [5].

USW is completed by the application of low amplitude high-frequency mechanical vibration to parts. Cyclical deformation of parts resulting from the mechanical vibration at the faying interface leads to heat generation due to intermolecular friction of polymer chains. The heat melts the polymer and connects the parts through fusion bonding. A general USW stack assembly is shown in figure 3. It houses a converter or transducer, booster, and a sonotrode also known as a horn [6]. The sonotrode (horn) transmits the vibration to the parts. The horn typically vibrates in the range of 20-40 kHz frequency and relatively low amplitudes of 50-200 μm_{p-p} [7]. This vibration between the faying surfaces generate frictional heat and causes surface melting at the interface. The two faying surfaces are then welded together through intermolecular fusion bonding [5].

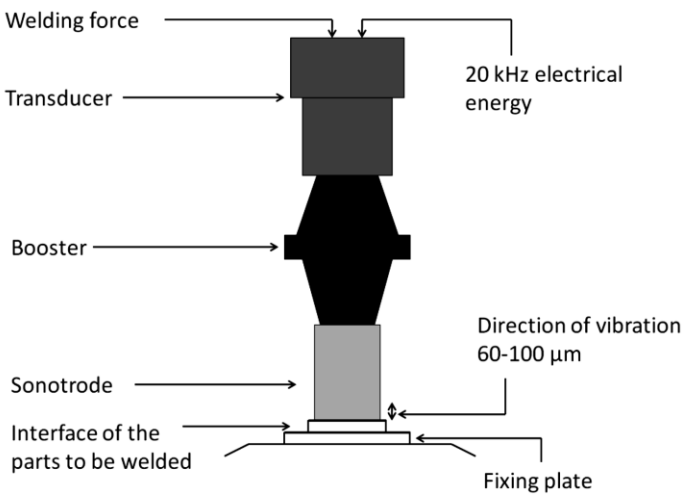

Figure 3. Components of a USW stack assembly [6]

To improve the consistency of the welded surface, a triangular protrusion is often molded into one of the two joining parts which is called an energy director or concentrator (Figure 4). The energy director causes the highest level of localized heating within the faying surfaces as a result of experiencing the greatest level of cyclical strain. Due to this effect, the protruded part melts and the surfaces are joined together [5]. The energy directors could also be molded in semicircular and rectangular shapes [8].

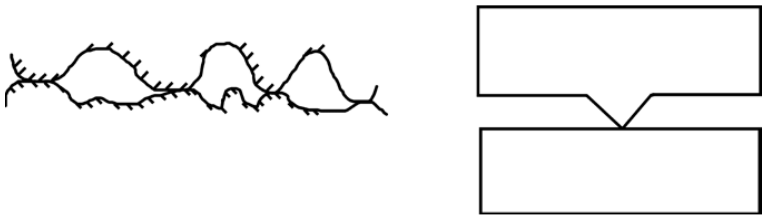

(a) (b)

Figure 4. Ultrasonic heating through cyclical deformation of (a) Surface asperities (b) Energy director [5]

A large number of thermoplastic and thermoplastic composites can be welded using USW. This welding method is economically feasible for mass production as the cycle time is very low. The cost of equipment will be justified as a high number of parts can be joined with

one system in a year. The whole welding cycle can be automated to further improve efficiency and lower the processing cost.

1.3. Effect of Moisture on FDM and USW

Moisture is an elusive detrimental factor when it comes to any form of polymer processing. FDM is more prone to moisture as in this process, the part is printed layer by layer. Within each layer, there are patterns in which air gaps exist. Moisture can easily diffuse into the air gaps and between layers if the parts are exposed to humid conditions. Also, if the filament is kept in room condition for a prolonged period, it absorbs moisture from the environment. As a result of using moisture loaded filament, the print quality, mechanical, and thermal properties of the part being fabricated could deteriorate. Kim et al. investigated the effect of moisture and temperature on the mechanical properties of ABS samples after manufactured by FDM and injection molding. The comparison between parts made from two processes showed that FDM parts absorbed water faster than the injection-molded ones. Both the tensile stress and young's modulus decreased with the increase in moisture [9]. In another study, specimens were printed from various ratio wood-PLA filaments first and then conditioned at different stages of relative humidity. It was discovered that the rate of moisture diffusion was higher in parts printed with filaments containing a higher content of wood. Moreover, diffused moisture in polymer filament tends to vaporize as it travels through the extrusion nozzle, causing morphological changes, bubble formation, and surface roughness in the printed parts [10]. Zaldivar et al. used ULTEM® 9085 filaments (blend of polyetherimide and polycarbonate), high-performance material mostly used in space applications. The focus of their study was to determine the effect of various filament moisture contents on 3D printed parts. Over the moisture contents, the tensile stress and failure strain were found to be decreased by more than 60% and 50% respectively. The increased

porosity and reduced glass transition temperature caused by moisture were found to be responsible for these significant changes [11].

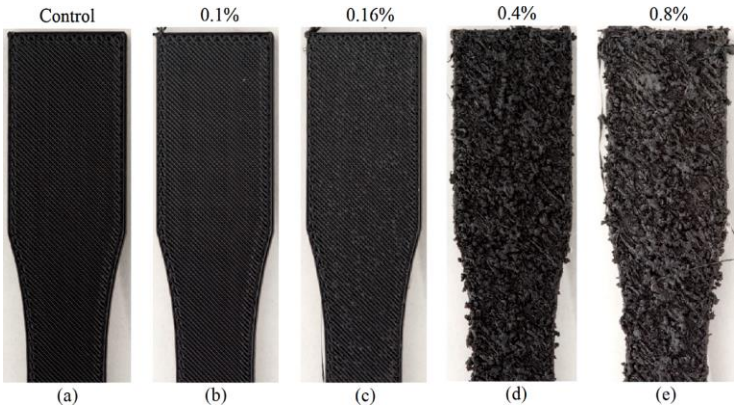

Figure 5. Negative impact of moisture on the surface quality of FDM parts [11]

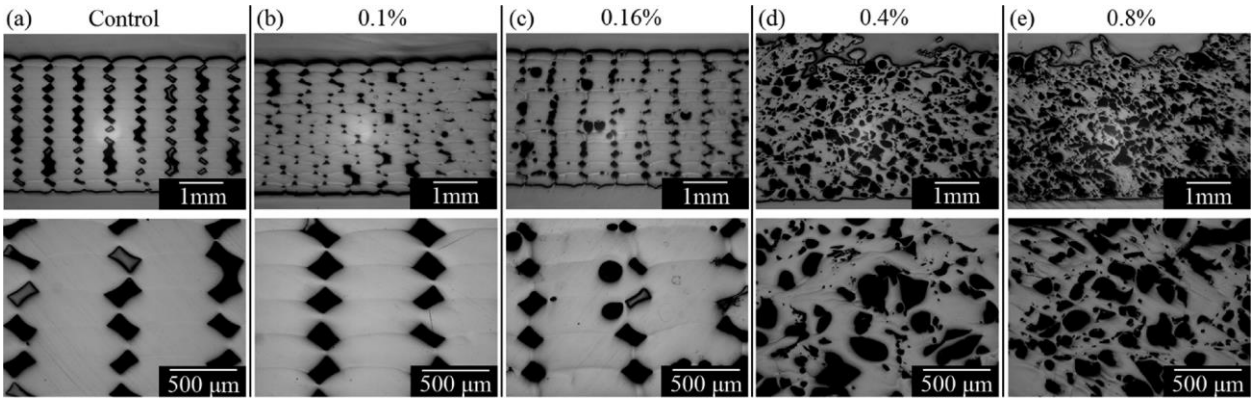

Figure 6. With increased moisture, the amount of porosity was increased as seen in the cross-section of FDM parts [11]

Moisture plays a crucial role in the weld quality of the mating parts during USW. Grewell et al. have shown that if moisture content within the parts exceeds above the allowed range, it will result in inconsistency in welding within parts of the same design specifications [5]. The presence of moisture alters the glass transition temperatures at the mating surfaces leading to variations in time for melting and fusion. This makes the intermolecular interaction between adjacent surfaces weak. The moisture on evaporation causes porosity at the weld seam which weakens the weld [12]. A few studies were conducted to investigate the effect of parts' moisture

on the weld characteristics. Liu et al. submerged the glass-fiber filled nylon-6 composite samples underwater for 24 hours and then dried the samples in a vacuum oven. The samples were removed from the oven at different times to induce the variability in moisture. USW was performed in these moisture variable parts and then parts were tested for tensile strength. It was reported that the weld strength decreased with increasing moisture content while the energy required for the welding also increased. It is an indication that keeping moisture at a minimum level could increase the joint strength and reduce the energy consumption of the welding system [8]. Hopmann et al. studied the impact of moisture on the welding of polyamide. They discovered that under a fixed set of welding parameters, the weld joint strength was reduced at higher moisture content (Figure 7). It was observed through microscopic imaging that gas bubbles were present along the weld seam and deduced that they were responsible for the reduction of strength [12].

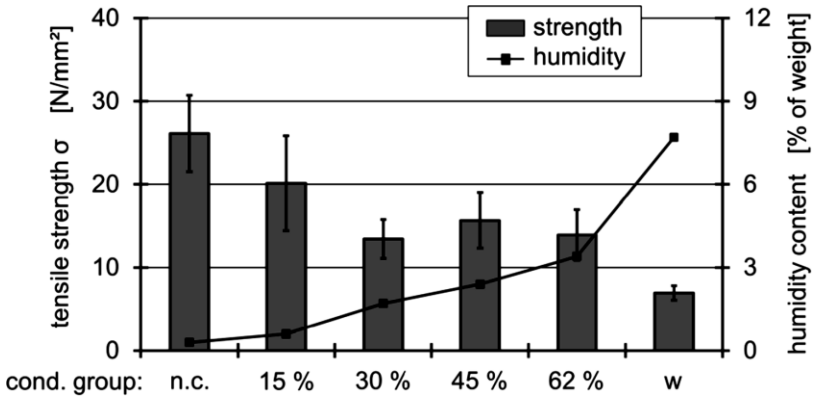

Figure 7. Weld strength decreasing with increasing humidity [12]

On the other hand, there are studies reported in literature discussing the effect of moisture on composites. For instance, the effect of moisture on the welding of polyamide 66 and carbon-fiber composite was investigated by Zhi et al. It was found that the water molecules broke the hydrogen bonds in polymer chains (Figure 8). As a result of this breakdown, the plasticization

characteristic and loss modulus of the composite was altered which caused the strength of the joint to decrease at high moisture intake [13].

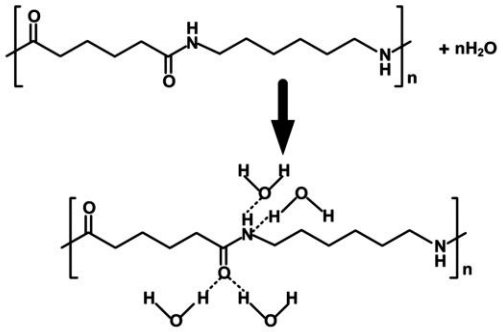

Figure 8. Water molecules breaking hydrogen bonds in polyamide 66 [13]

1.4. Motivation & Objectives

Though a large number of research studies have been published on the FDM of polymers, most of them focus on process optimization, composite filament development, reduction of anisotropic characteristics and other process parameter specific areas. There is very limited literature available on the moisture sensitivity of polymers during FDM. Moisture can be highly detrimental for some materials during FDM and can alter the mechanical and structural properties of the printed parts to a great extent. There is a good number of moisture sensitivity studies on injection molded and compression molded polymers and polymer composites. Christian et al. prepared biobased composites from plasticized cellulose acetate powder and poly(β-hydroxybutyrate) by using a hot press and studied the effect of moisture on uniaxial tensile properties [14]. Alvarez et al. utilized injection molding to produce samples by adding sisal fibers to a cellulose and starch-based commercial blend. The effect of both moisture and fiber content on the mechanical properties was studied [15]. In another study, slit extrudates were manufactured from poly(vinyl chloride) and wood sawdust by using a twin-screw extruder to study the effect of sawdust moisture content on the mechanical properties of the produced

composite [16]. Pan et al. experimented with starch and PLA blends to prepare injection molded composite specimens and studied the effect of moisture content on the tensile properties [17].

Kim et al. prepared the FDM samples first from ABS and then subjected them to moisture for a certain duration before mechanical property testing. They also studied the injection molded samples following the same procedure and compared the effects of moisture in both cases [18]. Filament moisture plays an important role in determining the mechanical, structural, and aesthetic qualities of an FDM printed part. Research regarding the effect of filament moisture on the mechanical property of FDM printed parts can be found in the works of Garces et al. [19] and Zaldivar et al. [11]. Apart from these two research studies, there are no known substantial research reports documenting the effects of filament moisture on FDM processed parts. So, it is crucial to understand the moisture absorption of filaments and its related impact on the mechanical property for both hygroscopic and hydrophilic polymers. PLA and PBS are two such biodegradable polymers that are currently used for a wide variety of applications. PLA/PBS composites are being developed for superior performance and new applications. PLA is popular in FDM but has some limitations concerning its elasticity. PBS is a new biobased plastic from the polyester family and has good flexibility, toughness, and biodegradable properties. PLA/PBS filaments for FDM could be one approach for addressing the limitations of PLA and producing high-quality outputs. Besides other aspects, the effect of moisture on the PLA, PLA/PBS blended filaments and on the parts printed from them needs to be studied in depth. Hence, the moisture sensitivity of PLA and PLA/PBS blended filaments are going to be characterized in this thesis.

USW of biobased polymers is relatively a new area of research. A few studies could be identified involving PLA, the most common bioplastic available but no other biopolymers or

bioplastics was studied for finding applications of USW. Stoehr et al. studied the weldability of neat PLA and plasticized PLA films for packaging applications. Polyethylene glycol was used as a plasticizer in that study. The authors investigated the effect of material composition on welding parameters for finding the most efficient setting. It was discovered that the plasticized PLA films could be welded at lower amplitude and higher welding force than the films without plasticizer. Also, the higher amount of plasticizer resulted in higher weldability of PLA films [20]. Vogel et al. also studied the USW of PLA films along with impulse welding. They discovered that by increasing the amplitude and weld force the failure load during tensile testing of the samples can be improved [21]. Kiss et al. explored the weldability of injection-molded pure PLA sheets through four different types of welding techniques. The results demonstrated that USW yielded the best efficiency and strength in joining the PLA specimens[22]. Lebron et al. worked with ISTeP, injection molded from PLA to develop a molecular diffusion model for the USW process. They experimented with amplitude, weld velocity, and weld distance to find out the respective impacts on mechanical properties [23]. This was the only study where the use of ISTeP parts for USW was found. There is no literature available regarding the moisture sensitivity analysis of PLA ISTeP parts during USW. Very limited studies were found characterizing the effect of moisture on the weld strength and other weld characteristics for polyamide, nylon, and some composite materials. Moreover, PBS was never used in any USW research. Besides, the PLA/PBS composite could be an alternative solution for a wide variety of applications. For these reasons, the USW of PBS, and PLA/PBS composite ISTePs need to be studied. Also, the effect of various humidity conditions on the weld strength and morphology of PLA, PBS, and PLA/PBS ISTeP need to be characterized.

Based on the above discussion, the objective of this thesis is divided into three parts-

Objective 1: Characterize the relationship between filament moisture content and tensile properties of PLA FDM specimens (chapter 2)

Objective 2: Characterize the relationship between filament moisture content and tensile properties of FDM specimens prepared from several PLA/PBS compositions (chapter 2)

Objective 3: Characterize the relationship between moisture content and ultrasonic weld strength of PLA, PBS, and PLA/PBS injection-molded ISTePs (chapter 3)

2. MOISTURE SENSITIVITY DURING FUSED DEPOSITION MODELING

2.1. Introduction

Among the available AM processes, FDM is the most popular method owing to its easier working principle and other associated advantages. A wide number of thermoplastic filaments are available for use in FDM to obtain specific output according to application. Composite filaments are also getting increased attention for special uses. But, the FDM process gets affected if the filament absorbs moisture. Moisture is responsible for many defects which can be prevented by drying the filaments or storing them in a controlled environment. Though the moisture absorption in filaments is a major problem plaguing the part quality in FDM, filament manufacturers do not provide any guidelines regarding proper storage. Hence, the moisture sensitivity of the filaments needs to be characterized to find out important information regarding storage and drying.

In FDM, material filament (predominantly polymers) is fed through an extruder that melts and pushes it throughout the nozzle on a build plate layer by layer. This process is favorable for the rapid fabrication of functioning prototypes and real scale parts. The FDM printers and materials are not very expensive and the process requires minimum monitoring after the initial process setting. It provides the flexibility of manufacturing geometrically complex parts with higher precision. The produced parts are lightweight, cost & time-efficient, and generate low process waste [24]. Several thermoplastics are commonly used in FDM among which PLA and ABS are the most popular ones.

Apart from PLA and ABS, polycarbonate, nylon, thermoplastic polyurethane, polyetherimide, polyether ether ketone are some of the other materials used in FDM [25]. Recently, lots of efforts are undertaken to produce new filaments by combining two or more

materials or reinforcing one material with fibers and/or additives. Of these newer combined materials, PLA and PBS combination has gained a lot of attention owing to their superior mechanical properties. PLA is strong, stiff, and brittle, it has mechanical properties in the range between polystyrene and polyethylene terephthalate [26]. It possesses great printability characteristics, good strength, and biodegradability [27]–[29]. But one of the limitations of PLA that curbs its widespread use is its brittleness. If the toughness of PLA can be improved by mixing with flexible polymers, the prospective applications can be greatly expanded [30], [31]. PBS has more ductility, flexibility, toughness, and properties similar to polypropylene but lacks rigidity [32]–[34]. The combination of these two materials could lead to high-performance, low-cost biodegradable composite filament. Unfortunately, PLA and PBS both are extremely moisture-sensitive materials.

Generally, hygroscopic and hydrophilic polymers are moisture-sensitive. These tend to absorb moisture from the environment. This absorbed moisture causes defects during the FDM process such as plasticization, degradation, bubble formation, microcracking, and hydrolysis resulting in increased porosity. Hence the moisture causes a detrimental effect on the mechanical properties of the final products [35]–[40]. To prevent this, drying of the material before FDM is recommended. Even though the manufacturers of commercial filaments provide drying temperature and durations they do not specify the frequency of drying or the favorable storage condition for filaments. As drying is an energy-intensive and thus expensive process, it is imperative to find out the acceptable amount of moisture in filaments without significantly reducing the mechanical properties of processed parts and the ideal storage condition to minimize drying frequency. Also, for any new composite materials, the characterization of moisture sensitivity and its respective effect on different properties is required before

commercial applications. In this study, moisture sensitivity of four PLA filaments and four PLA/PBS blend filaments is analyzed by characterizing the effect of moisture on mechanical, morphological, physical and thermal properties.

Filament moisture plays a negative role in determining several properties of final FDM parts. It is crucial to determine in what capacity the absorbed moisture is impacting the filaments. Based on this information, industrial as well as home users can determine their drying and storage conditions. The remaining of the paper is structured in the following way: section 2 describes the experimental methods thoroughly, section 3 provides the detailed results and discussion, and finally, the 4th section concludes the chapter.

2.2. Experimental Methods

2.2.1. Materials

Three different grades of Ingeo™ PLA filaments (4043D, 3D850, and 3D870) and PLA 2500HP pellets were supplied by NatureWorks LLC, U.S.A. BioPBS FZ71 (PTT MCC Biochem CO., Ltd., Thailand) was supplied by GC Innovation America.

2.2.2. Blend Preparation and Filament Processing

Before processing, drying was done in a convection oven to remove any moisture from PLA and PBS pellets. Drying was done at 50 ºC for 9 hours for PLA 2500HP and PBS pellets were dried at 80 ºC for a minimum of 5 hours. A co-rotating Leistritz twin-screw extruder was used to process FDM filaments from 100% PLA and four different PLA/BioPBS blends (90/10, 75/25, 60/40, and 25/75). The filament strands were passed through a water bath and then collected. Filament diameter was maintained in the 1.75±0.15 mm range to minimize the effect of under and over extrusion during the FDM process.

2.2.3. Differential Scanning Calorimetry

TA Instruments Q2000 was used to perform DSC. Samples weighing between 6-12 mg from each blend were sealed in an aluminium pan while a blank pan was used as the reference. The heat/cool/heat method was used to obtain the thermograms. The first heating cycle was started from 25 ºC with a ramp-up rate of 10 ºC/min up to 250 ºC under nitrogen gas. Then the sample was cooled down at 10 ºC/min to 25 ºC. The second heating cycle was carried out following the same parameters as the first one. TA Universal Analysis software was used to analyze the thermograms. The % crystallinity (X_c) of the PLA and PBS in the blends were calculated by using equation (1) and the values from the second heating curve [41].

$$X_c = \left(\frac{\Delta H_m}{W_f \times \Delta H_m^\circ}\right) \times 100\% \quad (1)$$

Here, ΔH_m and ΔH_m° are the melting enthalpy and 100% crystalline melting enthalpy. For PLA ΔH_m° is 93.0 J/g and 210 J/g for PBS [41], [42]. W_f is the weight fraction of the polymers in the blends.

2.2.4. Filament Cutting and Drying

Through trial printing, it was confirmed that 14 feet section of filament was needed to print one ASTM D638 type-IV tensile testing specimen. Based on this information, required 14 feet sections of filaments were cut from spools of the four different PLA grades and the four PLA/PBS blended filaments. Before each stage of moisture exposure, the filaments were dried according to the parameters in table 1. Even though the technical data sheet of 4043D recommended drying at 80ºC, filament deformation happened when the drying was attempted at that temperature. To prevent this, the temperature was lowered in steps to find out the suitable one for drying. It was noticed that at 50ºC the filaments were maintaining the original shape. For

this reason, drying was continued at 50ºC. The weights of the filaments after each drying were recorded to compare with the weights after moisture absorption.

Table 1. Drying parameters for different filament types

Type	Temperature (ºC)	Duration (hours)
3D850	80	4
3D870	50	8
4043D	50	4
2500HP	50	9
PLA/PBS	50	9

2.2.5. Moisture Conditioning

One set of filaments from each type of material were placed in a Binder KBF 115-UL humidity test chamber for one week at a specific temperature and RH for moisture absorption (figure 9). The temperature was set to 25 ºC and 50%, 65%, and 80% RH were maintained for a week for each level of humidity. To simulate the 100% RH scenario, the filaments were conditioned by submerging in a distilled-water filled container for one week. The weights of the filaments were recorded again after taking those out from the humidity chamber and percentage weight gain was calculated.

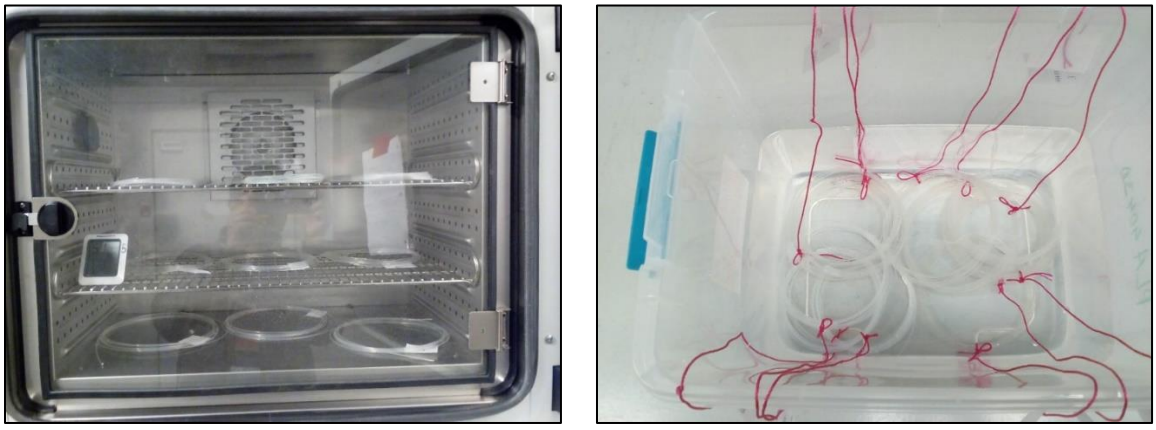

Figure 9. Moisture conditioning of filaments in a humidity chamber (left) and water for simulating 100% RH (right)

2.2.6. Fused Deposition Modeling

The FDM was performed with MakerBot Z18 desktop 3D printer. For the PLA filaments, a particular print setting was used while for the four PLA/PBS blends three different sets of print parameters were utilized to ensure high-quality output from each blend. The layer height, infill density, and infill pattern were set at 0.20 mm, 100%, and diamond respectively. The parameters which were changed from material to material is listed in table 2. with the values.

Table 2. Major FDM parameters for PLA and different PLA/PBS blends

Parameter	PLA	90/10	75/25 & 60/40	25/75
Extruder temperature	220 ºC	220 ºC	220 ºC	195 ºC
Chamber temperature	0 ºC	0 ºC	40 ºC	30 ºC
Retraction distance	1 mm	1 mm	1 mm	0.5 mm
Print speed	90 mm/s	50 mm/s	50 mm/s	18 mm/s
Raft to model vertical offset	0.40 mm	0.40 mm	0.50 mm	0.80 mm

2.2.7. Mechanical Testing

Instron universal testing machine 5567 was used for tensile testing of ASTM D638 Type IV specimens after FDM. A 30 kN load frame was used and the crosshead speed was set at 5 mm/min.

2.2.8. Scanning Electron Microscopy

Fracture surface morphology after tensile testing was observed using a JEOL JSM-6490LV scanning electron microscope. The fracture surface was sputter-coated with carbon and then placed inside the SEM chamber. 15 kV of acceleration voltage and several magnifications were used to capture the fracture surface images.

2.2.9. SEM Image Processing

To estimate the porosity percentages in the fracture surface SEM images, an algorithm was developed and programmed using latex. SEM image was first converted into the grayscale format. Then a Gaussian filter was applied to blur the pixels in the image. After that, each pixel is checked against a threshold value to compare whether the pixel value is less than the threshold value. This threshold value is defined as the ceiling function of the average of randomly selected four light gap pixels and four dark solid pixels. If a pixel is found below this value, the surrounding pixels were also compared. In case three surrounding pixels were also found to be below this threshold, the corresponding area was defined as a pore. Finally, the percentage of the porosity was calculated by dividing the total number of pixels in such pores by the total number of pixels in the SEM image.

2.2.10. Surface Roughness Measurement

Surfcom surface texture measuring instrument was used to measure the average surface roughness (R_a) of the top surfaces of the ASTM samples. Vertical magnification and cutoff were set at ×2K and 0.80 mm respectively while the measurements were recorded in microns (μm).

2.2.11. Tensile Testing of Filaments

To study the effect of moisture on the tensile property of the individual filaments, separate tensile testing was performed on Instron 5567 for PLA 4043D and PLA/PBS 75/25 filaments. The filaments were tested with specially designed tensile testing grips and a 2 kN load frame. 50 mm/min crosshead speed, and 150 mm gauge length was used.

2.2.12. Melt Flow Index of Filaments

The MFI of the PLA and PLA/PBS filaments subjected to tensile testing was measured after moisture conditioning at different RH levels. At the end of moisture conditioning, the

filaments were pelletized. MFI testing was performed using Custom Scientific Instruments MFI2-156 Melt Flow Indexer and following ASTM D1238 guidelines (210 ºC/10 kg).

2.2.13. Statistical Analysis

Two-way ANOVA was performed on the maximum tensile stress and % elongation values of all PLA grades and PLA/PBS blend samples. A two-sided confidence interval with $\alpha = 0.05$ was used. Tukey Post-hoc analysis was also done to find out the effect of each humidity level on the tensile stress and % elongation of each particular filament type. A two-sided confidence interval with $\alpha = 0.05$ was used for the post-hoc analysis. All analysis was performed using Minitab 18 statistical software.

2.2.14. Prolonged Moisture Exposure

For observing the long-term effect of moisture on the tensile properties of FDM printed parts, four PLA grade filaments were placed in room condition for three months. Cutting, drying and weighing was performed by following the same procedure used during one-week moisture exposure. After three months, the filaments were weighed again and ASTM D638 Type IV samples were printed. Finally, tensile testing of the samples was performed using the Instron load frame.

2.3. Results and Discussion

2.3.1. Thermal Properties

Thermograms from the DSC are displayed in figure 10 and the thermal properties are listed in table 3. With the increase of PBS content in PLA/PBS blends, the glass transition temperature (T_g) of PLA decreased. The T_g of PLA dropped from 62.01ºC for neat PLA to 58.03ºC in PLA/PBS 25/75 blend. The melting point (T_m) of neat PLA was also reduced from 175.56ºC to 174.65ºC in PLA/PBS 25/75 blend [41], [43].

Table 3. Glass transition, melting temperature, melting enthalpy, and % crystallinity of PLA/PBS blends

PLA/PBS blend ratio	T_g of PLA (ºC)	T_m (ºC)		ΔH_m (J/g)		X_c (%)	
		PLA	PBS	PLA	PBS	PLA	PBS
100/0	62.01	175.56	-	16.61	-	17.86	-
90/10	60.21	175.16	112.68	44.95	1.32	5.27	0.62
75/25	60.51	175.75	112.82	33.45	2.87	4.61	0.53
60/40	60.14	175.51	113.11	29	13.67	6.19	1.94
25/75	58.03	174.65	113.51	12.15	43.0	4.62	2.42
0/100	-	-	113.42	-	64.42	-	30.68

Only PLA/PBS 25/75 blend exhibited double melting peaks in the thermogram. This behavior was also observed in the works of Qahtani et al., Yoo et al., and Wang et al. This phenomenon can be attributed to the melting, recrystallization, and remelting of two kinds of crystal formation during the cooling phase. The first melting peak was due to the melting of imperfect crystals and the second one was when the more organized crystals melted at higher temperatures [41], [44], [45].

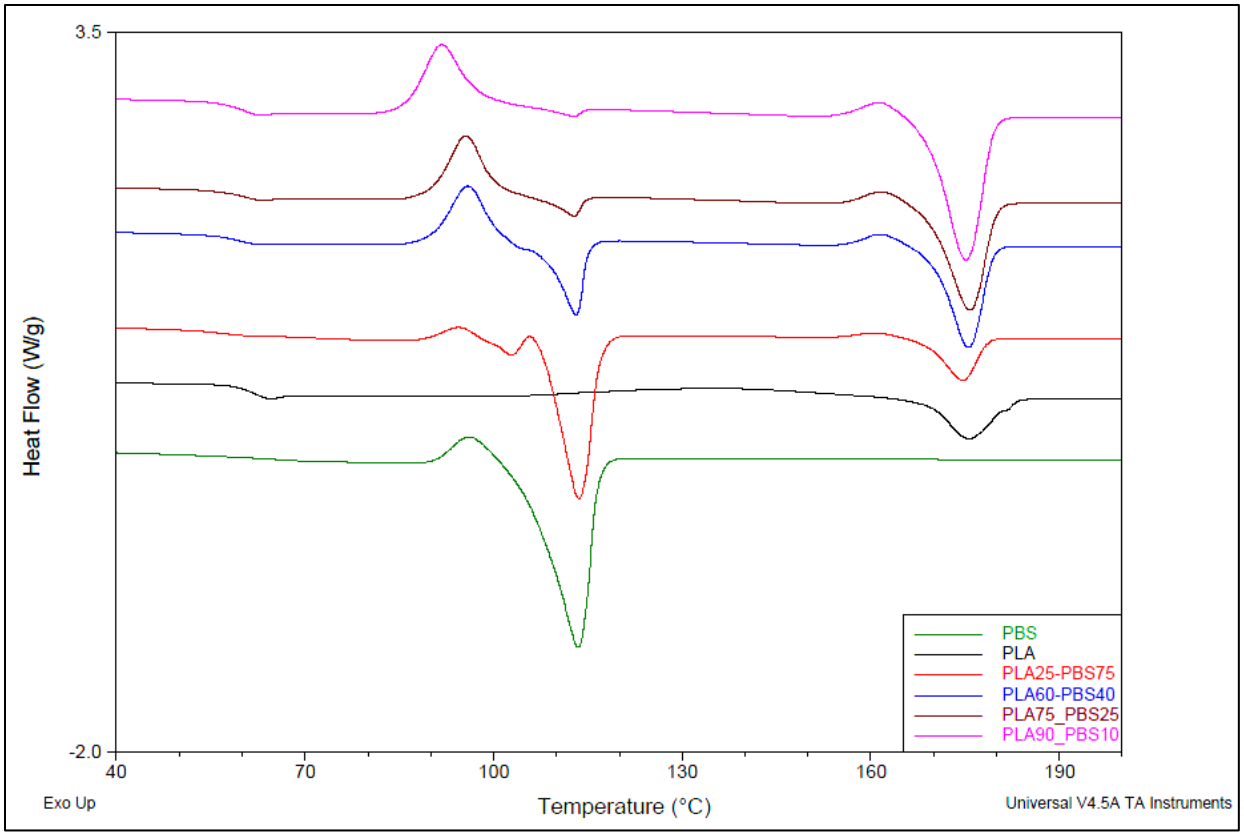

Figure 10. Thermograms of PLA/PBS blends obtained from DSC

2.3.2. Weight Gain of Filaments

Figure 11 illustrates the percentage weight gain of the PLA and PLA/PBS blended filaments after moisture conditioning for one week respectively. At 50% and 65% RH, 3D870 had the highest weight gain of 0.40% and 0.45% respectively. 4043D had the highest weight gain of 0.73% at 80% RH and 3D850 gained the most weight in water submerged conditions. For the PLA/PBS blends, 75/25 filaments had gained the most weight in water submerged conditions. Also, the weight gain % of 25/75 blends was increased exponentially.

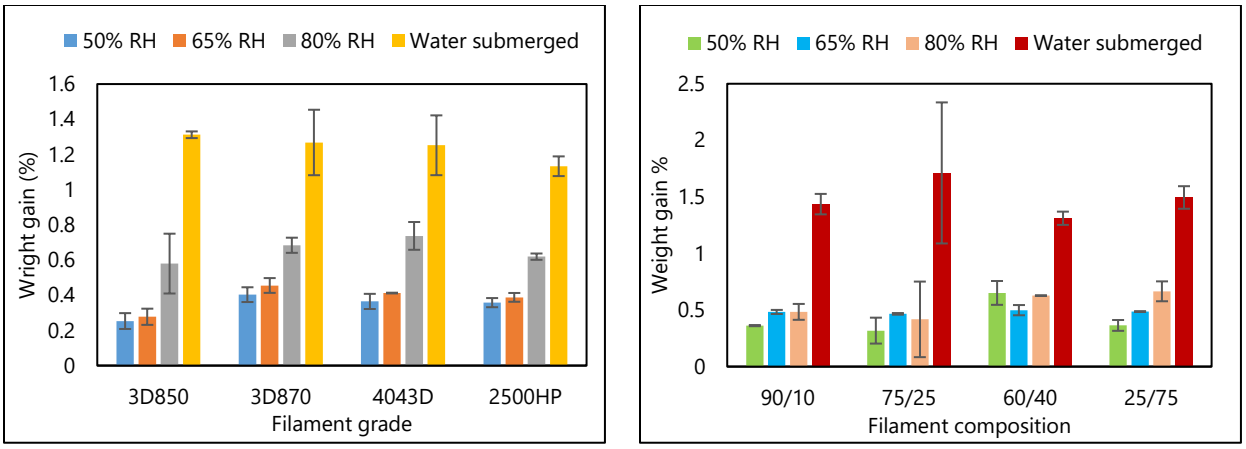

Figure 11. Weight gain % of PLA (left) & PLA/PBS filaments (right) (Error bars show standard deviation)

2.3.3. Tensile Properties

Tensile testing results of the 3D printed PLA samples are displayed in figure 12. Two-way ANOVA analysis showed that filament grade, humidity level, and their interaction have a significant effect on both the maximum tensile stress and % elongation of PLA samples. One-way ANOVA and Tukey Post-Hoc analysis was performed to determine the effect of each humidity level on the tensile stress and % elongation of a particular filament type. Out of four, the maximum tensile stress and % elongation of only one grade-PLA 4043D was significantly affected by humidity level. In general, among the four PLA grades, 4043D had the lowest tensile stress and % elongation values. From figure 12 it can be noticed that the maximum tensile stress of 4043D samples for dried, 50%, and 65 % RH are within a maximum range of 3.73% of one other. But with 80% RH and water submerged samples, it reduced drastically. In 1-Week of observation, 4043D was the most resilient against up to 65% RH level. %D-lactide content could be the reason behind the tensile properties observed in 4043D. D-lactide and L-lactide are isomers of lactide. They are mirror images of one another and cannot be superimposed on top of another. In D-lactide, the methyl group is positioned above the plane of the screen. While the

other three grades of filaments have only 0.5% D-lactide, 4043D has 4.3%. High D-lactide impacts the crystallization and thermomechanical behavior of PLA greatly. It causes slow crystallization and lowers the maximum achievable crystallinity along with the melting point [46]. We assume that the high %D-lactide could be allowing the moisture to impact the mechanical properties of 4043D at high RH levels. 3D870 had the second-lowest tensile stress but in terms of % elongation, it had the highest values. Both 3D850 and 2500HP had similar tensile properties. The tensile stress of 2500HP samples have increased with moisture but this can be attributed to the diameter variation of in-house made filaments. The inconsistent diameter caused over extrusion during 3D printing and resulted in differences in tensile stress. A similar phenomenon was observed by Ang et al. where the micro gaps between the printed lines were filled due to over-extrusion of material and it overlapped to a greater than recommended level for rigid filaments [47].

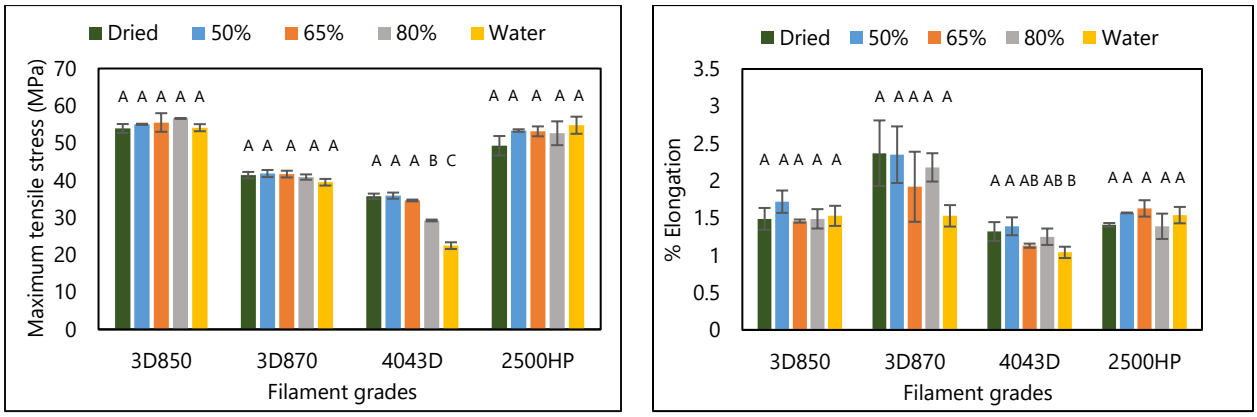

Figure 12. Maximum tensile stress of four PLA grades samples (left) & % elongation of four PLA grade samples (right) (Error bars show standard deviation)

Tensile properties of samples prepared from PLA/PBS filaments are presented in figure 13. Two-way ANOVA analysis showed that both the material composition, humidity level, and their interaction have a significant effect on maximum tensile stress but only the material composition has a significant effect on % elongation. Tukey Post-Hoc analysis was performed on

the individual groups of PLA/PBS blends to identify any significant effects on the tensile stress and % elongation. It was observed that the maximum tensile stress of both PLA/PBS 75/25 and 25/75 specimens were significantly affected by the humidity levels. % Elongation was not significantly affected by humidity levels at all. With the increase of PBS content in the PLA/PBS blends, the tensile stress became lower. This reduction in the tensile stress with the increase in PBS content could be explained by the immiscibility and phase separation between PLA and PBS. Several researchers have reported that PLA/PBS blends are not miscible and phase separation happens when PBS content exceeds a certain percentage. Bhatia et al. used modulated DSC to confirm that these two materials are immiscible but their rheological results displayed compatibility while there was less than 20% PBS in the blend [48]. Jompang et al. reported that PLA is miscible with PBS when it was added up to 10% with PLA [49]. Phase separation in PLA/PBS blends was reported in the works of Deng and Thomas where they observed co-continuous phase separation in blends having more than 8.4 wt % PBS and stated that PLA and PBS are thermodynamically incompatible [50]. In our study, we processed PLA/PBS blend filaments up to 40% PBS without any visible phase separation issues. But during the FDM processing of PLA/PBS 25/75 filaments, extreme warpage was observed. We hypothesize that the phase separation between PLA and PBS is dependent on the material grades being used and that could be the reason behind the differences in % PBS content responsible for phase separation cited in literature.

On the other hand, as PBS is a ductile material, the increase of PBS content in PLA/PBS samples led to higher % elongation values. Ou-Yang et al. worked with several PLA/PBS blends and observed the same trend in their results [19]. It should be noted here that, for PLA/PBS 25/75 blend, the material exhibited high warpage during 3D printing even after reducing the print

speed and cooling rate to a greater extent. Ou-Yang et al. observed the same phenomenon when working with a blend having more than 80% PBS. This warpage was the result of thermal stress buildup due to shrinkage of volume during cooling [51]. It could be the reason for high standard deviation and inconsistent trends in mechanical properties of the PLA/PBS 25/75 blend.

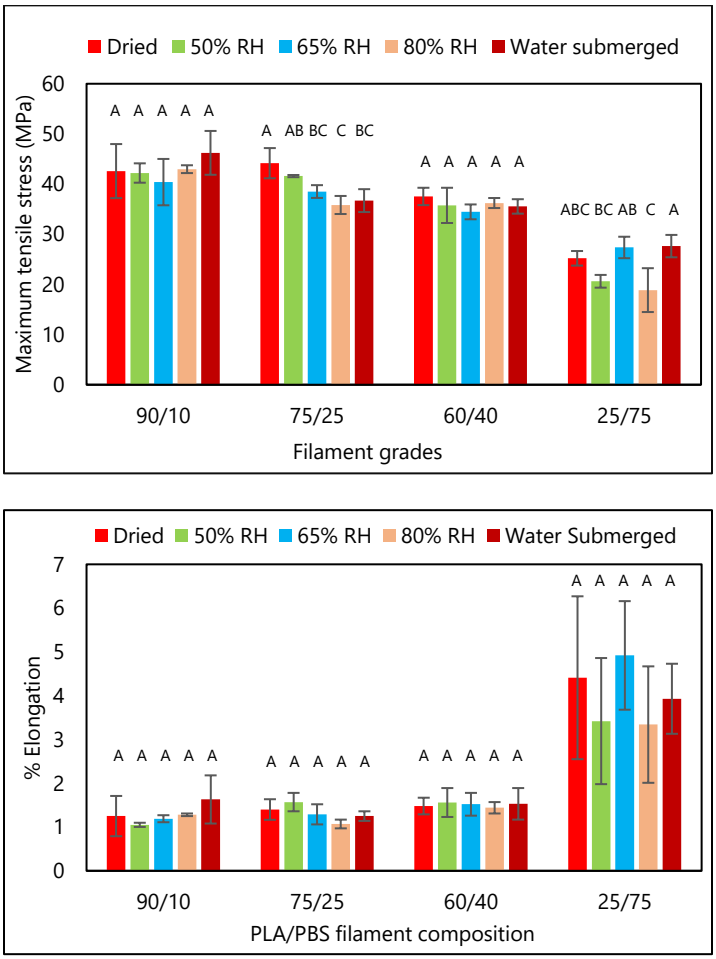

Figure 13. Maximum tensile stress (top) & % elongation (bottom) of four PLA/PBS blend FDM samples (Error bars show standard deviation)

2.3.4. Fracture Surface Morphology

As the tensile properties of PLA 4043D was significantly affected by moisture conditioning, the fracture surfaces of 4043D from four different RH levels were examined through SEM and the observed images are displayed in figure 14.

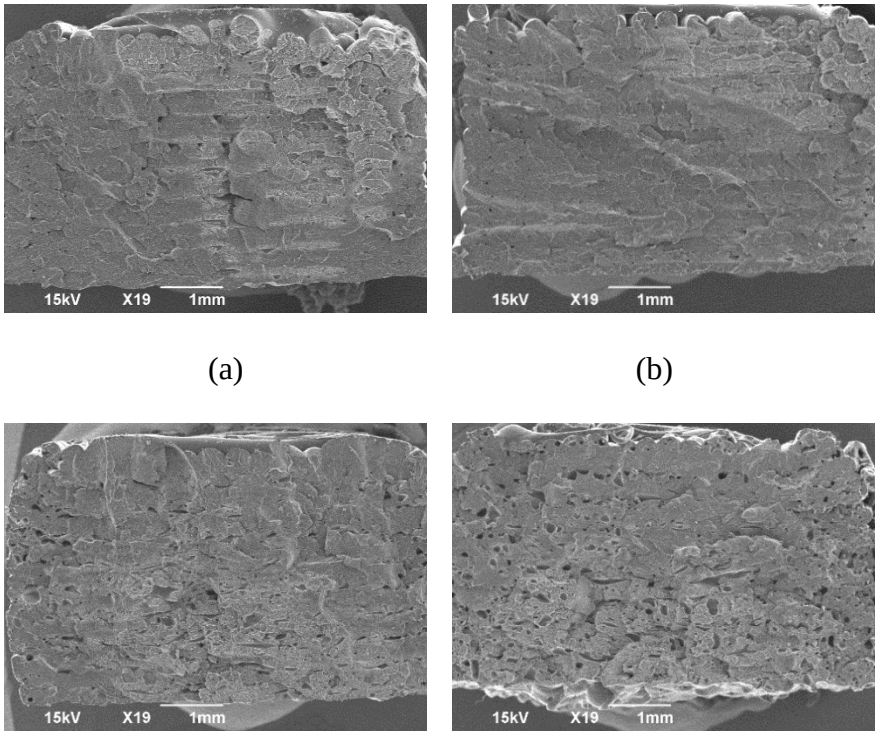

Figure 14. SEM images of 4043D fracture surfaces (a) dried (b) 50% RH (c) 80% RH (d) Water submerged samples

It can be noticed that with the increase of RH, the level of porosity increased in the samples. Specifically, in 80% and water submerged samples, the porosity content was very high. Moreover, the individual layers were unidentifiable in samples conditioned at an RH of 50% and greater but could be distinctly noticed in dried samples. Zaldivar et al. studied the effect of initial filament moisture on parts printed from ULTEM® filaments. Increased porosity in the cross-section of parts printed from high moisture content (0.40% and 0.80%) filaments were observed. Also, they observed a decrease in the viscosity of the material with the addition of just 0.1% water in the filaments and noticed a more compacted cross-section which helps to explain the layer overlapping phenomenon that we observed in our study [11]. The increase in porosity at high RH corroborates the negative effect of moisture on the tensile properties of 4043D printed

samples. Increased porosity resulting from the increase in RH significantly lowered the maximum tensile stress and % elongation for 4043D.

In Figures 15 and 16, a few sample PLA/PBS fracture surface images are shown. From the analysis of the images, no relationship between RH level and porosity was observed. There was no significant presence of porosity in the fracture surfaces of ASTM fabricated from four PLA/PBS blends.

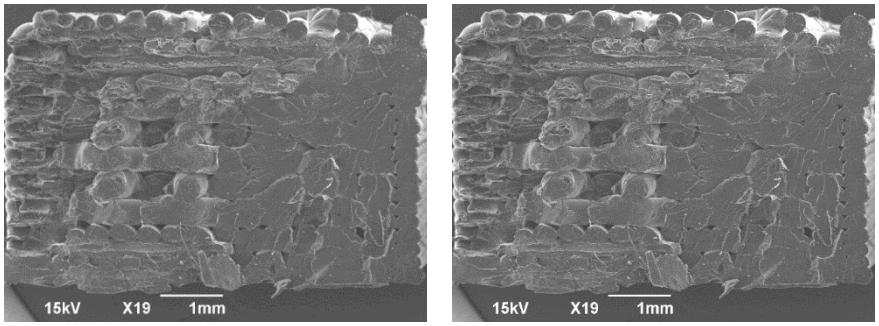

Figure 15. SEM images of PLA/PBS fracture surfaces: 75/25 dried (left), 75/25 water submerged (right)

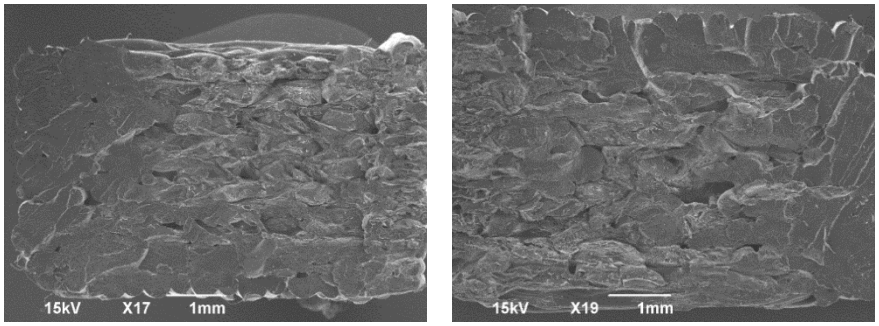

Figure 16. SEM images of PLA/PBS fracture surfaces: 60/40 dried (left), 60/40 water submerged (right)

2.3.5. Porosity Measurement in Fracture Surface

The porosity from the fracture surface images of PLA 4043D subjected to different RH levels was estimated as percentage porosity by using the above-described algorithm. Figure 17 displays raw images and the respective processed images with calculated porosity %.

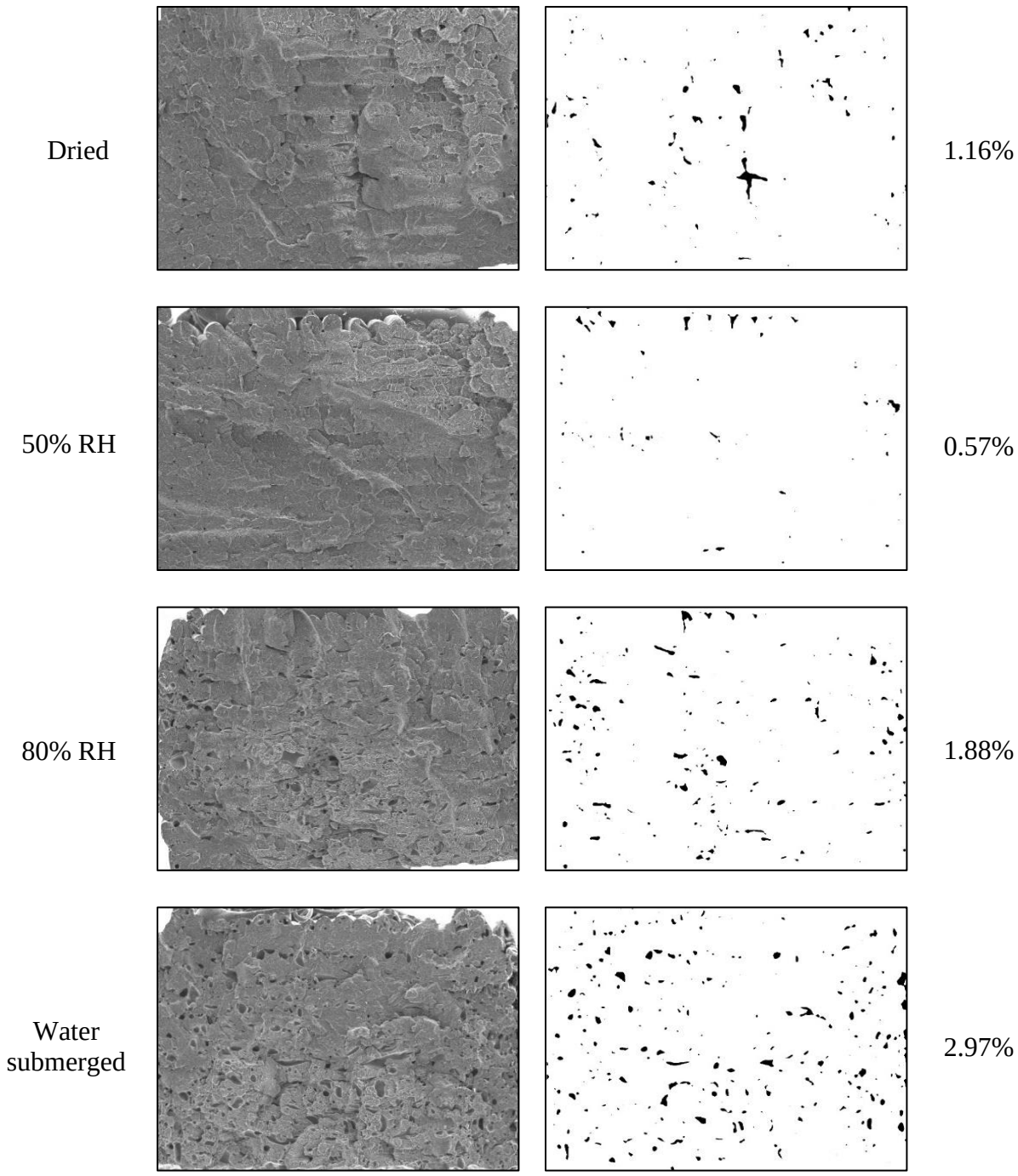

Figure 17. % Porosity estimation through image processing of SEM fracture surfaces (Texts on the left side indicates the RH levels of the filaments and on the right side indicates the estimated % porosity)

The proposed algorithm is not very robust as it is susceptible to color gradient across the image. The threshold value for identifying the pores was set by using a trial and error procedure

till the most accurate approach was finalized. For example, in the processed image of the dried sample, a relatively large area was captured as porosity but in actuality might be due to the nature of the fracture in the visualized plane. While capturing a 3D surface as a 2D image, the height differences of the planes in the fracture surface may create a false positive visualization of a porosity like defect. Leveling the fracture surfaces through polishing before image processing could be an approach to identify the pores more accurately. The algorithm could be further improved by using machine learning on a large data set and training the program to detect pores more efficiently, accurately, and capable of distinguishing the true pores from the pores resulting from height differences which we could not achieve due to limitations with the available time and data.

2.3.6. Print Surface Characterization

Figure 18 shows the average surface roughness values for four PLA grade filaments obtained using the surface profilometer. Tukey Post-Hoc analysis showed that only the surface roughness of 4043D was significantly affected by different moisture conditions. It can be noticed that the roughness of the 50% and 65% RH samples are much lower than all the other samples. This could be attributed to the MFI of the filaments during FDM. The stepped surface finish which is a characteristic of FDM parts could be the reason behind the high roughness values in dried samples [52]. As the molten material maintained a streamlined flow and was deposited uniformly in dried samples, high roughness values were observed. With the increase of RH to 50% and 65%, the MFI of the molten polymer increased which is explained in the following section. The higher MFI might have caused the deposited material to flatten a little more than the original elliptical shape [53] during deposition and produced lower roughness values. The exposure to the high RH of 80% and water submerged conditions have increased the MFI further

(figure 22) and causing the material to flow quicker. As a result, the polymer might have been deposited erratically creating uneven surfaces which yielded higher surface roughness values.

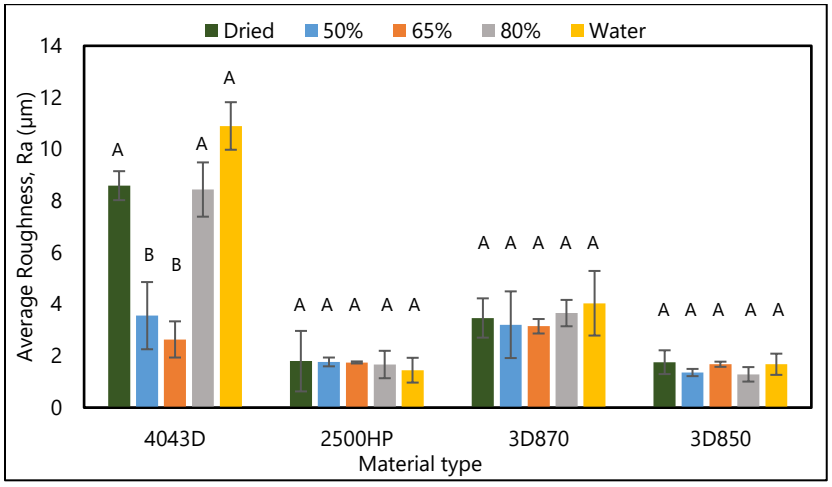

Figure 18. Average surface roughness of PLA samples under different moisture conditions (Error bars show standard deviation)

Tukey Post-Hoc analysis of the surface roughness values from PLA/PBS blend samples showed that no values were significantly affected by the different humidity levels (figure 19). Also, the surface roughness of PLA/PBS samples is much higher than the surface roughness of PLA samples. As PLA and PBS are both semi-crystalline and are thermodynamically immiscible at higher blend ratios of PBS, the higher surface roughness observed in the blends may be due to the difference in crystallinity after phase separation during cooling.

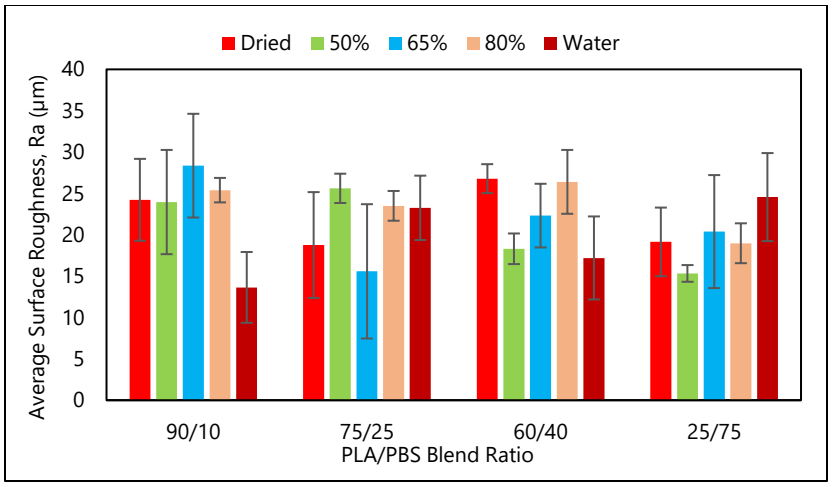

Figure 19. Average surface roughness of PLA/PBS ASTM samples from different humidity levels

2.3.7. Filament Tensile Test and Melt Flow Indexing

The results from the tensile testing of PLA 4043D filaments after moisture conditioning is displayed in figure 20. The maximum tensile stress of the filaments reduced with increased moisture condition and the % elongation increased. This result is in correlation with the results from the tensile properties of 3D printed samples.

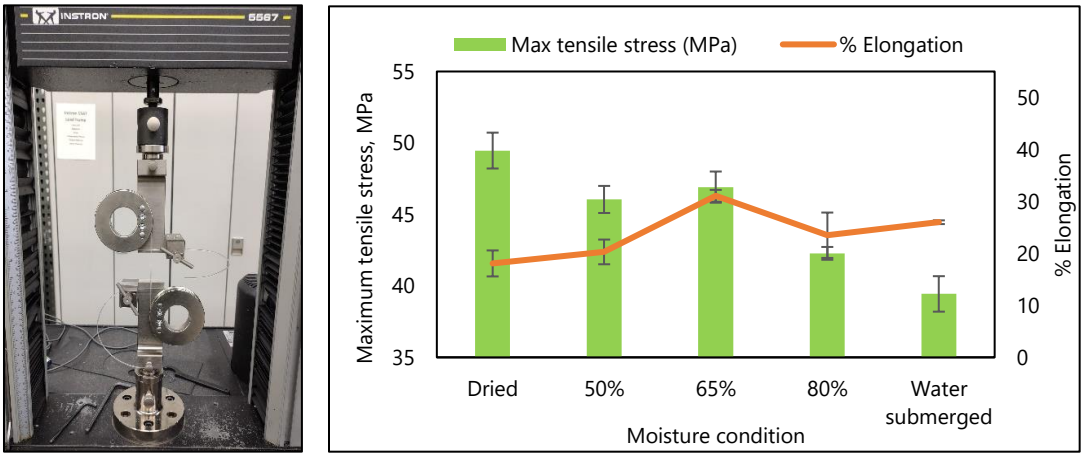

Figure 20. Tensile test setup (left) and tensile properties (right) of PLA 4043D filaments after conditioning at different RH (Error bars show standard deviation)

Figure 21 shows the tensile properties of PLA/PBS 75/25 blended filaments after moisture conditioning. There were no major differences in the strength of the conditioned

filaments as the standard deviation of the observed values overlapped with each other. This could be because of the diameter variation of in-house made PLA/PBS filaments. But the % elongation seemed to have increased with the increase in moisture.

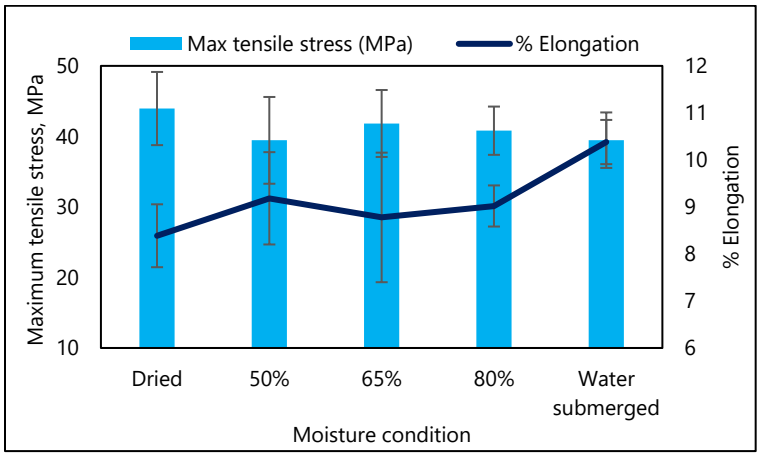

Figure 21. Tensile properties of PLA/PBS 75/25 filaments after conditioning at different RH (Error bars show standard deviation)

The effect of moisture on the melt flow behavior of the polymers was found out from the MFI testing. Figure 22 displays the MFI of PLA 4043D and PLA/PBS 75/25 filaments after one week of moisture conditioning at respective parameters. It can be noticed that the MFI of both of the materials became higher with increased RH. Similar observations were recorded by Zaldivar et al. where the MFI of ULTEM® 9085 was increased by 1 gm/10 min from control specimen to 0.20% moisture content specimen [11]. For PLA 4043D, the general trend is the increase of MFI with moisture. A small decrease in the MFI for water submerged samples was observed but the value was within the standard deviations of the 80% RH MFI and might be attributed to the machine inaccuracy. PLA/PBS 75/25 filaments had higher MFI than PLA in general and an upward trend was observed. With these MFI results, the surface roughness discrepancy of 4043D became clear. Our hypothesis regarding the role of MFI on the roughness values was true and the MFI results confirmed this.

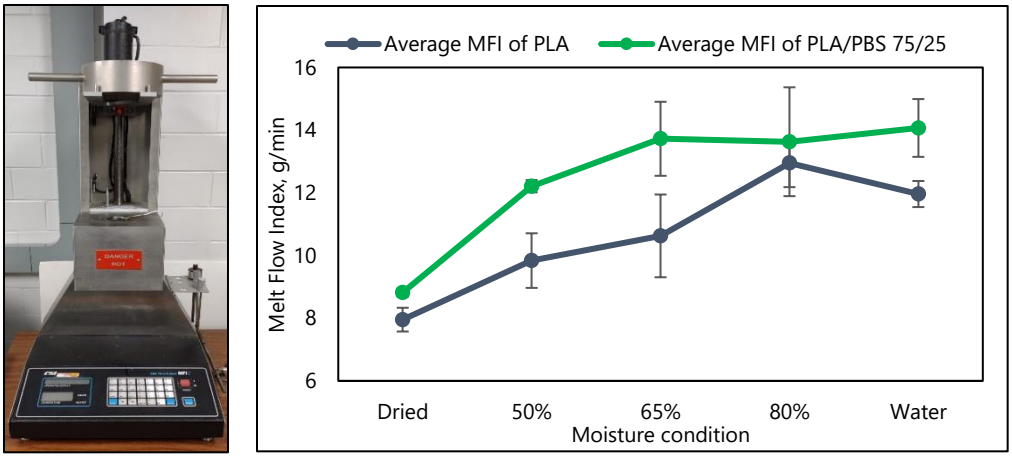

Figure 22. MFI of PLA 4043D and PLA/PBS 75/25 blend filaments at different moisture conditions (Error bars show standard deviation)

2.3.8. Effect of Prolonged Moisture Exposure

Figure 23 displays the weight gain % of 50% RH, water submerged (from one-week duration), and three months moisture exposed filaments.

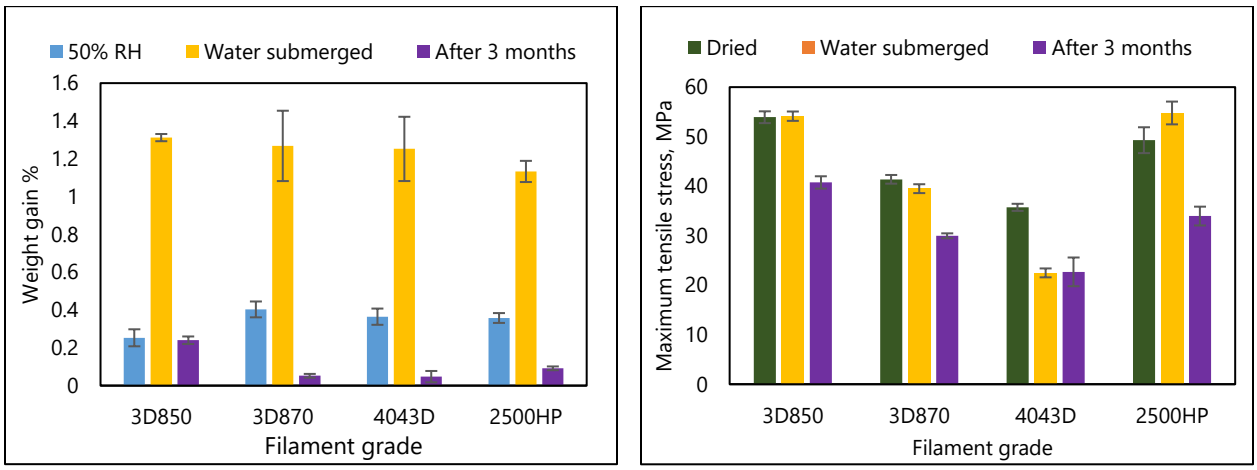

Figure 23. Weight gain % (left) and maximum tensile stress (ASTM) of dried, water-submerged, and 3 months room condition filaments (right) (Error bars show standard deviation)

It also illustrates the maximum tensile stresses of the ASTM samples from the dried, water submerged, and three months conditions. From the figure, it is evident that the weight gain of the filaments after 3 months in room condition is minimal but its effect on the tensile stress was very significant. Apart from 4043D, the maximum tensile stress of the other grades was

reduced to a larger extent. This shows that storing filaments in room condition for a long period reduces the tensile stress of the printed parts drastically even if the absorbed moisture content is insignificant. We hypothesize that over this longer duration of exposure to environmental moisture, the core structures of the polymer chains hydrolyze, weakening the capability to deliver maximum part strength in FDM. In addition to that, it also informs us that placing filaments in high RH for one week would result in a high weight gain. But the high weight gain might not affect the tensile property of samples in the same way for all grades of filaments.

2.3.9. Drying and Storage

From the results presented above, it is evident that up to 65% RH, the tensile stress variation was minimal in the conditioned ASTM samples. For PLA 4043D, at or above 80% RH, the impact of moisture on maximum tensile stress was extreme. For the PLA/PBS 75/25 blends, the moisture conditioning above 50% RH had lowered the strength to a higher extent. The % elongation of filaments, as well as MFI after moisture conditioning, displayed an upward trend with increased moisture for both 4043D and 75/25 blends. Based on these observations, it is our recommendation to store the filament spools at room condition (25˚C/50% RH) to ensure standard quality in printed parts. The filaments could be stored in room condition for up to 7 days before drying is needed again. As for the drying, we completed a reverse drying experiment where a set of 4043D filaments were first dried completely and then conditioned at various RH levels. The weight before and after conditioning was recorded. The conditioned filaments were then dried again following the parameters in table 1 and checked for weight loss after specific times have passed. It was found that more than 90% of the gained weight was lost after the drying took place for the prescribed duration (figure 24). Hence, the manufacturer recommended drying temperature and duration were applicable for most of the grades tested except PLA

4043D. The deformation of 4043D filaments at the manufacturer recommended temperature compelled us to lower the drying temperature from 80°C to 50°C and the reverse drying test proved our initiative as an effective one.

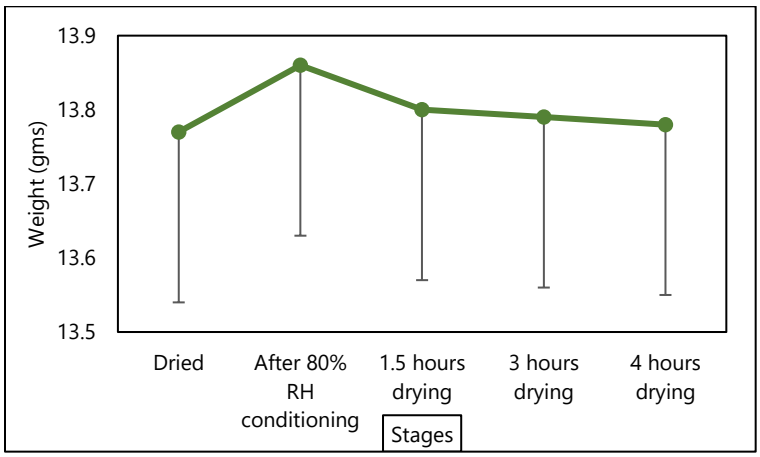

Figure 24. Average weight of 80% RH filaments at different stages (Error bars show standard deviation only in the negative direction)

2.4. Conclusion

Moisture sensitivity of four PLA filaments and four PLA/PBS blend filaments were studied after conditioning at different RH and testing for tensile, physical, thermal, and flow properties. Completely dried filaments were conditioned at 25˚C temperature and 0%, 50%, 65%, 80%, and 100% RH levels for one week before FDM printing. Tensile testing of PLA ASTM samples revealed that PLA 4043D is more sensitive to moisture than the three other filaments and both the tensile stress and % elongation were severely impacted at high humidity levels. A high level of porosity was observed in the fracture surfaces of samples printed from 80% and 100% RH filaments. An image processing algorithm was developed and applied on the 4043D fracture surface images to calculate the percentage of porosity. The calculated porosity relatively represented the number of pores in the fracture surfaces and corresponded well with the observed porosity. But the algorithm could be improved further for higher accuracy in future.

Moreover, the surface roughness measurement of PLA ASTM samples had shown that 4043D exhibited a high degree of variation in response to changes in RH. Among the four PLA/PBS blends, the maximum tensile stress of 75/25 and 25/75 samples were significantly affected by moisture. The 25/75 blend showed extreme warpage during FDM and proved that PLA and PBS are not thermodynamically compatible with each other at high PBS content. Based on the tensile property results, filament tension testing and melt flow indexing were conducted on the two most impacted materials-4043D and PLA/PBS 75/25. The filaments were conditioned using the same settings mentioned above. The % elongation of the filaments displayed an upward trend while maximum tensile stress showed a downward trend with the increase in moisture. The MFI of both materials had also surged up after each stage of moisture exposure. The tensile testing of samples printed from three months room conditioned filaments produced an extreme reduction in maximum tensile stress than we observed for a one-week duration. This displays the adverse effects of moisture on printed parts because of storing the filaments for a long duration in room condition. The weight gain % was very low but the effect of environmental moisture was the opposite in that situation.

Our work provides the researchers, commercial filament manufacturers, and general FDM users a step-by-step guideline on carrying out moisture sensitivity analysis of materials and the associated experiments to characterize the effect of moisture. It also presents the differences in mechanical properties when filaments are exposed to different RH levels for a short term. Moreover, the long-term effect of filament storage in room condition was studied and the results were found to be significantly different from the short-term conditioning. In the future, mathematical modeling of moisture diffusion behavior could be carried out to predict the diffusion into the filaments. The stereochemistry of polymers after being exposed to moisture for

an extended period and the respective effect on various mechanical characteristics could be another research prospect. Detailed rheological experiments and analysis were not considered in our study which can also be included.

3. MOISTURE SENSITIVITY DURING ULTRASONIC WELDING

3.1. Introduction

Ultrasonic welding is a widely used secondary processing technique in industries for joining parts produced from thermoplastics and thermoplastic composites. It is performed by applying high frequency & low amplitude mechanical vibrations to the connecting parts. The major advantages of this welding technique are low cycle time, ease of automation, relatively low initial capital, and could be tailored to weld various types of thermoplastics. It is mainly used for parts that are difficult to mold as one piece due to design constraints or cost [5].

Many thermoplastics can be welded using ultrasonic vibration. ABS, acrylic, polyamide, polycarbonate, polystyrene, nylon, polyethylene terephthalate, polyetheretherketone, polyethylene, polypropylene are the most common thermoplastics used in USW. It can be applied to weld dissimilar thermoplastics. Grewell et al. provided an in-depth weldability analysis and reference guide regarding the ease of joining different thermoplastic materials in separate welding situations [5].

In the last decade, USW of PLA has increased exponentially due to the excellent weldability and widespread use of PLA in a large number of consumer products such as packaging sheets, films, and injection molded components. As a biodegradable, environment-friendly alternative to petrochemical thermoplastics, the use of PLA and the USW of PLA had seen a substantial increase. On the other hand, polybutylene succinate (PBS) is a relatively new biodegradable material from the polyester family. The application of PBS is expanding as more research on different applications are being completed but the major use of PBS right now is in the food packaging field. The composition of PLA and PBS at different ratios could lead to improved properties and new applications. PLA/PBS blend processing, methods for improving

compatibility, corresponding toughness, crystallization, degradation, and recycling behaviors along with applications of PLA/PBS blends have been well documented in the literature [54]–[59]. The prospect of PLA/PBS blend is high as the previous works stated several benefits and commercial applications of the PLA/PBS blends.

Despite the focus on PLA/PBS blends and PBS for numerous applications, the ultrasonic weldability analysis of these two types of materials is not yet conducted extensively. Moreover, being hygroscopic materials, PLA and PBS absorb moisture quickly. Most of the time after primary processing (injection molding) the parts are stored in an uncontrolled environment or without proper guidelines to protect them against moisture. USW which is a surface mating process might not take place immediately after primary processing. As a result, moisture diffusion into the surface occurs over an extended period. The absorbed moisture could impact the weld quality and strength largely. Hence, moisture sensitivity of PLA, PBS, and PLA/PBS blends during USW needs to be characterized.

In this paper, ISTeP was prepared from 100% PLA, 100% PBS, and PLA/PBS 25/75 blends. The parts were exposed to several moisture levels before USW and then tested for weld strength. Statistical analysis was performed to isolate any significant effects of moisture on the weld strength. Fracture surface morphology was examined to identify the respective effects of moisture differences.

3.2. Methodology

3.2.1. Materials

PLA 2500HP pellets were acquired from NatureWorks LLC, U.S.A. BioPBS FZ71 (PTT MCC Biochem CO., Ltd., Thailand) was procured from GC Innovation America.

3.2.2. Blend Preparation and ISTeP Molding

Three different PLA/PBS blends 75/25, 50/50, and 25/75 were prepared using a Leistritz Twin Screw extruder. Temperatures ranging from 290˚F to 380˚F was used starting from zone 1 to zone 7 of the extruder to prepare the blends. The compounded materials from three blends and virgin PLA, PBS pellets were sent to a contract manufacturing company to manufacture ISTePs. The company have the mold for ISTeP caps and cups and is the official supplier for Dukane Ultrasonics Inc. Out of the five material types, the ISTeP molding was successful only for three- 100% PLA, PLA/PBS 25/75, and 100% PBS. PLA/PBS 75/25 ISTeP caps had ejector pin-push and sink marks on them. The 50/50 ratio blend had produced worse defects than 75/25. The ISTePs from the remaining three blends had minimal defects. 100% PBS caps and cups had dome-shaped surfaces on the top and bottom of the parts respectively (figure 24). The dome-shaped protrusions were removed by manual sanding using sandpapers. As the mold was machined by considering the properties of polycarbonate, it was not fully suitable for molding the PLA/PBS blends.

Figure 25. Dome-shaped protrusion on 100% PBS cup

3.2.3. Moisture Conditioning of ISTePs

Before the conditioning of ISTePs, they were dried in a convection oven at 50˚C for a minimum of 9 hours. Binder KBF 115-UL humidity test chamber was used to condition the

ISTeP parts for one week. The temperature was kept constant at 25˚C and RH was set at 50%, 65%, and 80% to condition the caps and cups in three consecutive weeks. All three types of ISTeP caps and cups were placed inside the test chamber at the same time. The dried caps and cups were considered as 0% RH samples and to simulate the 100% RH, the parts were submerged in a distilled water-filled container for a week at room temperature. The weight of the caps and cups were recorded before and after the moisture conditioning.

3.2.4. Ultrasonic Welding

After the moisture exposure was completed, the caps and cups were immediately welded using a Dukane iQ Servo Ultrasonic Welding system. It is rated to 20 kHz weld frequency and is equipped with patented melt-match® technology. Before the final welding stage, a series of trial welding experiments were performed to fine-tune the different weld parameters. PLA ISTeP caps and cups were used for the trial runs. Different levels of trial parameters were tested until a target of getting an even weld area without any flashes was achieved along with checks for any surface deformities on the top of caps. The levels and ranges of parameters were chosen based on expert opinions from Dukane Ultrasonics. To prevent the rotation of parts in the fixture cavity after ultrasonic vibration is applied, a circular piece of cork padding was placed inside the cavity (figure 25).

Figure 26. Cork-padding in fixture cavity to prevent rotation of parts

Based on the trials, the final weld parameters were selected as mentioned in table 4

Table 4. Finalized ultrasonic weld parameters in iQ Explorer II software

Parameter	Value
Booster	1:1
Horn	1:1.5
Trigger force	200 N
Weld distance	0.30 mm
Weld velocity type	Segmented
Weld velocity	0.20 mm/s to 0.80 mm/s in 8 segments

Using the above values for the parameters' listed welding was performed on all parts conditioned under different RH levels.

3.2.5. Pull Test

Pull test of the welded samples was completed using an Instron load frame. Customized pull test fixture (figure 26) and adaptor were machined to use the fixture in a 30 kN load frame. The test was performed at a linear crosshead speed of 3 mm/min. The weld area of the test samples was determined by substituting the values of the inside diameter, d_i and the outside diameter, d_o of the round hollow cylinder-shaped ISTeP cups in equation 2.

$$A_w = \pi \left(\frac{d_0}{2}\right)^2 - \pi \left(\frac{d_i}{2}\right)^2 \quad (2)$$

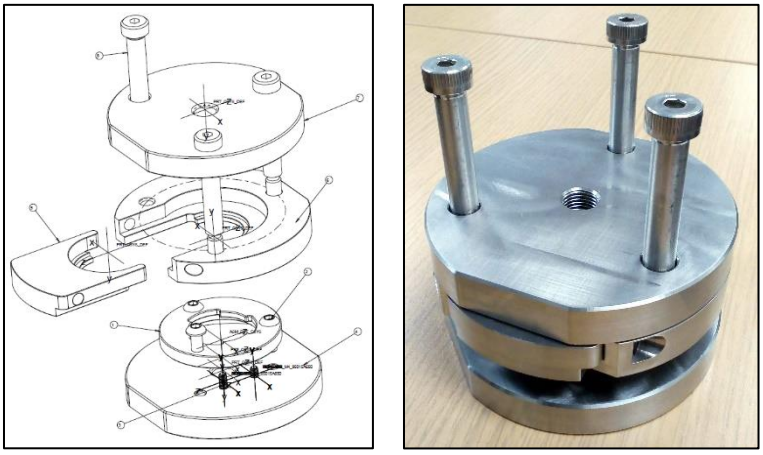

Figure 27. Drawing of the pull test fixture (left) and machined fixture (right)

3.2.6. Scanning Electron Microscopy

Fracture surface morphology of the designated weld areas from both caps and cups after pull testing was observed using a JEOL JSM-6490LV scanning electron microscope. First, the specific sections of the weld area were cut before the fracture surface was sputter-coated with carbon and then placed inside the SEM chamber. 15 kV of acceleration voltage and several magnifications were used to capture the fracture surface images.

3.2.7. Statistical Analysis

Two-way ANOVA was performed on the maximum weld strength and % elongation values for all types of ISTePs. Tukey Post-hoc analysis was performed to determine the effect of humidity level on the weld strength and % elongation. A two-sided confidence interval with $\alpha = 0.05$ was used in both cases. All analysis was performed using Minitab 18 statistical software.

3.3. Results

3.3.1. Weight Gain

The weight of the caps and cups before and after moisture conditioning were recorded and displayed in figure 27. For 100% PBS and PLA/PBS 25/75 caps, the moisture absorption behavior was similar except in the case of water submerged conditions. 100% PBS caps gained much higher weight. 100% PLA caps gained higher weight than the other two material types at 50% and 65 % RH but less weight at 80% RH and water submerged condition.

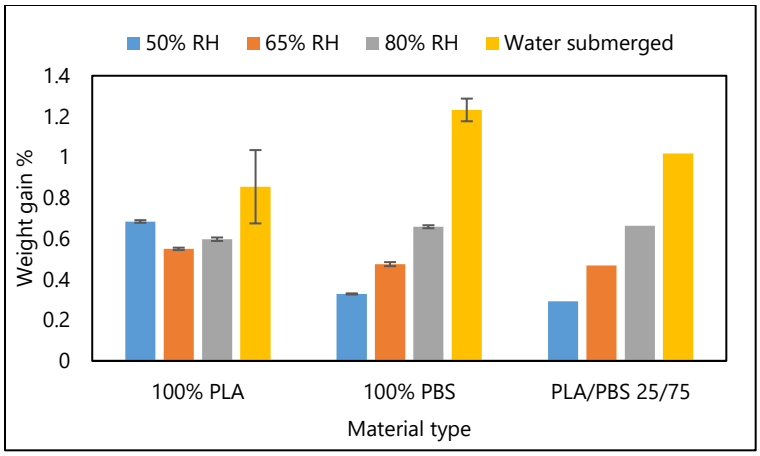

Figure 28. Weight gain % of caps after conditioning at different RH levels

Figure 28 shows the weight gain % of ISTeP cups. At 50%, 65%, and 80% RH the weight gain behavior in all three material types are relatively similar. In the water submerged condition, the highest weight gain was observed in 100% PBS and the lowest in 100% PLA. Based on the information presented, it can be inferred that at high RH levels, the 100% PBS and PLA/PBS 25/75 injection molded ISTeP parts are more sensitive to moisture. But the weight gain % of the 100% PLA caps and cups show relatively smaller differences from each other over the different RH levels.

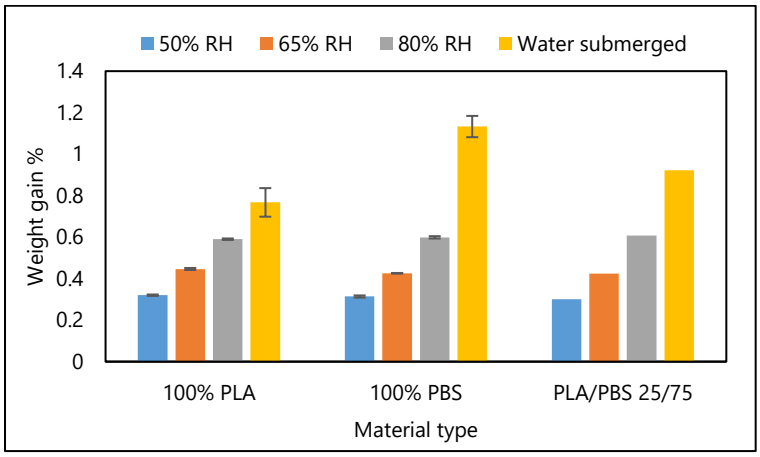

Figure 29. Weight gain % of cups after conditioning at different RH levels

3.3.2. Mechanical Properties of the Ultrasonic Weld

USW was performed on the ISTeP parts after moisture conditioning and subsequent weighing. The pull test was performed following the USW to determine the mechanical properties of the weld joint. The test information is illustrated in figure 29. Two-way ANOVA analysis showed that both material type and RH level significantly affected the maximum weld strength of the samples. For % elongation, material type, humidity level, and their interaction significantly affected the values. One-way ANOVA and Tukey Post-Hoc analysis was performed to determine the effect of each RH level on maximum weld strength and % elongation of each type of material.

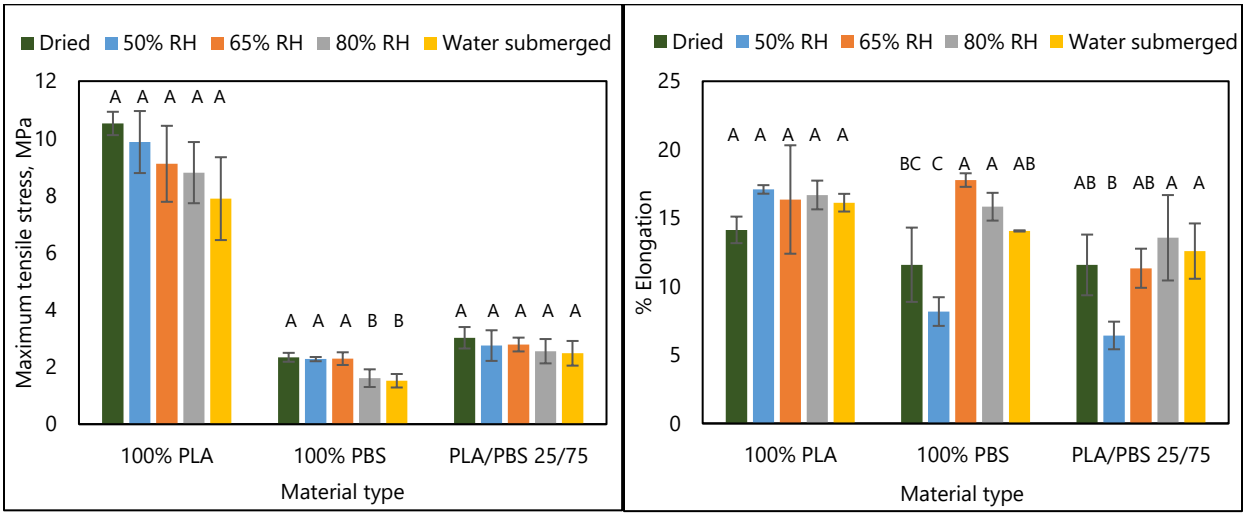

Figure 30. Maximum weld strength (left) and % elongation (right) of three kinds of ISTePs

It was observed that the humidity level did not significantly affect neither maximum weld strength nor % elongation of 100% PLA ISTePs. On the other hand, 100% PBS ISTePs' maximum weld strength and % elongation was significantly affected by the change in humidity levels. While the weld strength of PLA/PBS 25/75 was not significantly affected, the % elongation was influenced significantly by the change in humidity level.

3.3.3. Fracture Surface Morphology

Before performing the pull test on the welded samples, a random section of each ISTeP was marked to create a reference point for observing in scanning electron microscopy after the pull test is completed. From each material and moisture condition, the respective reference area of the fracture surfaces from a few caps and cups were observed. The SEM of dried and water submerged PLA ISTePs are displayed in figure 30

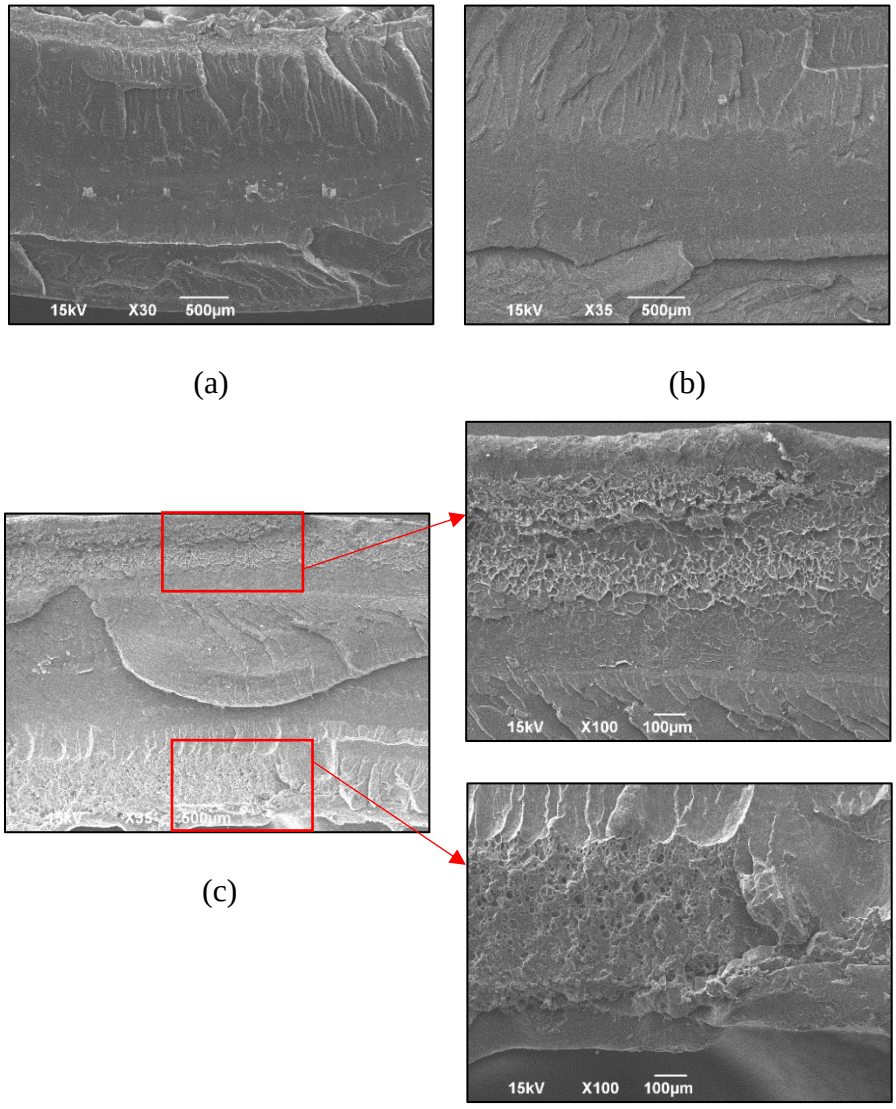

Figure 31. SEM images of 100% PLA weld area after pull testing for (a) Dried cap (b) Dried cup and (c) water submerged cap

From the dried cap and cup images, it can be noticed that the weld area had a clean brittle fracture and no noticeable pores are present. But in the water submerged caps, we can identify some trapped pores along the boundary of the weld joint. The area inside the red squares are magnified and the porosity can be seen more clearly. The presence of porosity along the boundary of the weld area in water submerged samples is a result of the heat generated during the application of ultrasonic vibration. This heat is insufficient to remove the existing moisture. The moisture gets trapped in the molten material, creating porosity, and weakening the weld joint as indicated by the downward trend of maximum weld strength for 100% PLA in figure 20.

PLA/PBS 25/75 dried and 80% RH ISTePs are shown in figure 31. There are no signs of porosity in the weld area of dried cups whereas a high degree of porosity was observed in 80% RH caps and cups.

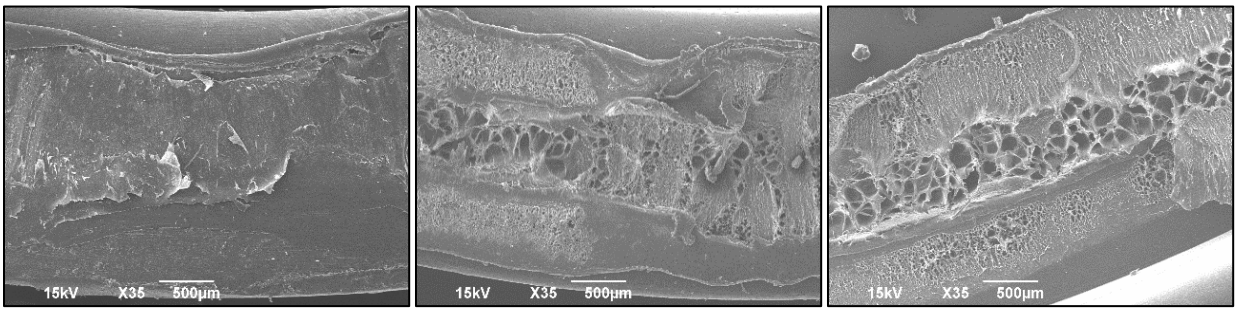

Figure 32. SEM of weld area for PLA/PBS 25/75 ISTePs: Dried cup (left), 80% cup (center), and 80% cap (right)

The air bubbles created due to porosity are larger than the ones present in PLA ISTePs. At the 100µm scale, the porosity in PLA can be hardly seen but at the 500µm scale, the porosity in PLA/PBS ISTePs could be seen very clearly. This could be an indication of PLA/PBS 25/75 being more moisture sensitive than 100% PLA. Figure 32 represents the SEM images of the 100% PBS ISTePs from dried and water-submerged conditions.

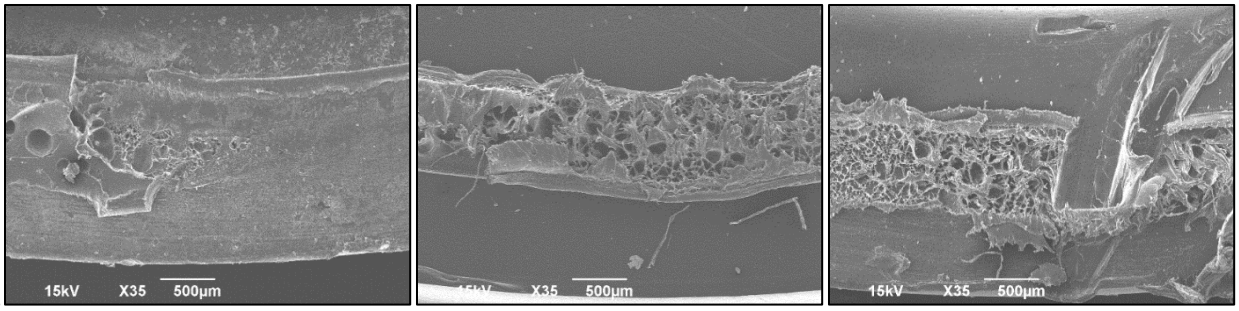

Figure 33. SEM of weld area for 100% PBS ISTePs: Dried cup (left), water submerged cap (center), and water submerged cup (right)

Similar to PLA/PBS 25/75 ISTePs, porosity was present largely in the high RH samples but not in dried ones. The water submerged samples displayed large air bubbles trapped in the weld surface and the fracture surface shows signs of ductile fracture which could be due to the ductile nature of PBS.

3.4. Discussion

To study the effect of moisture on ultrasonic weld strength of PLA, PBS, and PLA/PBS ISTeP parts, we performed a moisture sensitivity experiment. ISTePs from three types of materials were conditioned at five different RH levels and tested for weld strength. We observed a reduction of weld strength and an increase in trapped porosity at the weld seam for all ISTePs made with PLA, PBS and PLA/PBS at higher RH levels. Similar results were observed by Zhi et al.[13]. They have studied the effect of moisture on the weld and morphological properties of carbon-fiber and polyamide 66 composites. It was observed that the absorbed moisture changed the plasticization property of the composites by breaking the hydrogen bonds in polymer chains which in turn reduced the weld strength at high moisture content. An increased number of voids was also found in the fracture surfaces of the high RH samples.

We hypothesize that, in our study, the absorbed moisture hydrolyzed the polymer structure at the faying surfaces and altered the plasticization and melting characteristics. Upon

heat generation through ultrasonic vibration, the absorbed moisture tried to evaporate away but the generated heat was not high enough to remove the moisture in the very short weld time. As a result, moisture was trapped in the form of air bubbles in the weld seam which was observed in the SEM images. Similar results were observed in other polymer-moisture sensitivity studies as explained in the following paragraph.

It was reported by Hopmann et al. that the absorbed moisture tends to evaporate away due to heat generated by applied ultrasonic vibration. But due to incomplete evaporation of moisture, porous structures are generated at the weld seam weakening the weld [12]. Liu et al. worked on USW of glass-fiber filled nylon composites and performed a moisture sensitivity study. The samples were tested for joint strength after different amounts of moisture were exposed to the samples. The joint strength of the nylon composites was reduced with higher moisture content and welding energy requirement increased [8]. The effect of moisture on the lap shear strength of ultrasonically welded carbon/nylon composites was reported by Liu et al. [60]. The strength reduced exponentially with increase in moisture content. This reduction was attributed to the reaction between water and amide molecules and the resulting weakening of hydrogen bonds. The reduced weld strength observed in ISTeP samples made with different types of polymers in our study can be attributed to the cumulative impact of the above-discussed phenomena.

3.5. Conclusion

Through our study, it is evident that PBS and PLA/PBS ISTePs can be ultrasonically welded. We characterized the effect of one-week moisture exposure (five different humidity levels) on the weld strength and morphology of the parts. Moisture played a detrimental role in the joint strength of ISTeP parts. A downward trend was observed in weld strength of100% PLA

ISTeP parts while weld strength of 100% PBS ISTeP parts was significantly affected when RH was above 65%. SEM images of the weld areas after the pull test showed an increase in the amount of porosity in samples conditioned at higher RH levels compared to the dried ones. In the future, weld parameter optimization of 100% PBS and PLA/PBS ISTePs could be explored to obtain a higher weld strength. Also, the effect of long-term moisture exposure (few months) could be included.

4. SUMMARY

4.1. Significant Results

In this thesis, the moisture sensitivity of PLA and PLA/PBS blends were studied for both FDM and USW. In FDM, four grades of PLA filaments and four PLA/PBS blend filaments were conditioned at five different RH conditions before printing ASTM D638 Type IV samples. The tensile testing of printed ASTM samples was performed and it was determined that the tensile stress of PLA 4043D and PLA/PBS 75/25 samples was decreased with the increase in moisture. Statistical analysis also showed the significant effect of moisture on the tensile stress for these two materials. To characterize this deduction further, filament tension test and MFI test were performed for these two specific filament types after moisture conditioning at the same RH levels as the previous set of experiments. Melt flow behavior of the filaments was highly impacted by moisture exposure and the tensile property was also decreased with increase in RH. For 4043D, the tensile stress decreased from ~50 MPa to ~40 MPa from dried to water submerged condition while the MFI increased from ~8 gm/min to ~12 gm/min over the same conditions. MFI of PLA/PBS 75/25 also increased from ~9 gm/min (dried) to ~14 gm/min (water submerged). To observe the long-term influence of moisture, the same four PLA grade filaments were stored in room condition for three months and then printed using the same configuration of FDM parameters as used in the previous experiment. Tensile testing was performed on the 3-month conditioned sample to determine the tensile properties. It was observed that, over the prolonged duration, environmental moisture affected the filaments profoundly and the tensile stress was reduced by a large extent. For instance, in 3D850 and 3D870 samples, the tensile stress decreased by ~24% when compared with the test results of 1-week water submerged samples. For USW, we planned to prepare ISTeP from three different PLA/PBS blends along

with 100% PLA and 100% PBS were made by injection molding. Out of the total five, 100% PLA, 100% PBS, and PLA/PBS 25/75 were successfully molded. The ISTeP caps and cups were moisture conditioned at five different RH conditions before USW. After welding, pull testing was performed to observe the effect of moisture on weld strength. It was noticed that the weld strength of 100% PBS was significantly affected above 65% RH while a downward trend was found in the strength of 100% PLA and PLA/PBS 25/75 ISTePs with increasing RH levels. % Elongation of PLA/PBS 25/75, and 100% PBS was also significantly affected by moisture. The SEM images of the weld area after pull testing showed trapped porosity. The results from the FDM and USW section of this study indicate that exposure to moisture for a few days can impact the outcome of the processes greatly. We can deduce that if the parts were exposed to moisture for a longer duration, the weld strength would decrease even further. Compiling the results from all the experiments performed in this thesis together, we were able to characterize the sensitivity of moisture on PLA, PBS, and PLA/PBS composite parts during FDM and USW.

4.2. Future Directions

In this thesis, the scope was limited to capturing the moisture sensitivity at chosen levels of RH for PLA, PBS, and PLA/PBS composite parts during FDM and USW. In future studies, different levels of moisture exposure and the relationship with different process parameters can be studied. In the following two paragraphs, we have discussed few possible directions that the study could progress. In the first paragraph, additional experimentation that can be performed using the FDM process is discussed and in the following paragraph, we have discussed experimentation concerning USW.

From the FDM perspective,

1) Detailed rheological experiments and analysis of moisture conditioned filaments could be considered. The changing viscoelastic characteristics of different materials under different RH situations could be better understood through this approach.
2) The stereochemistry of polymer chains could be studied to discover chemical changes in core structures of polymers due to moisture conditioning.
3) To predict the moisture diffusion in a particular material, mathematical modeling of diffusion behavior could be another project. The diffusion coefficient and other associated factors could be included in the development of the model.
4) The relationship between filament moisture, FDM process parameters, for example, layer height, infill density, infill pattern, and mechanical properties of the printed samples could be explored.

From the USW perspective,

1) The welding parameter optimization of PLA/PBS 25/75 and 100% PBS could be an approach. In the current study, same weld parameters were used for welding three types of materials as our scope did not include determining the best weld parameters for every material.
2) The investigation regarding any relationship among weld energy, power, and force required for welding different materials could be carried out. The hypothesis of parts moisture impacting the required weld power, energy, and force could be tested too.
3) The effect of long-term (few months) moisture exposure on weld strength for the materials used can be studied.

4) As the ISTeP injection molding of two PLA/PBS blends was not successful, the process improvement of the two blends could be undertaken to ensure better results in injection molding.

REFERENCES

[1] ISO, “Additive Manufacturing-General Principles—Part 1: Terminology,” *ISO/DIS 17296-1 2014*, 2014.

[2] J. P. Kruth, “Material Incress Manufacturing by Rapid Prototyping Techniques,” *CIRP Ann. - Manuf. Technol.*, vol. 40, no. 2, pp. 603–614, 1991.

[3] R. Daniele, “Polymer composites for sustainable 3D printing materials,” Doctoral thesis, Department of Materials, Mechatronics, and Systems Engineering, University of Trento, Trento, Italy, 2019. Accessed on: September 2, 2021. [Online]. Available: http://eprints-phd.biblio.unitn.it/3813/

[4] K. V. Wong and A. Hernandez, “A Review of Additive Manufacturing,” *ISRN Mech. Eng.*, vol. 2012, pp. 1–10, 2012.

[5] D. A. Grewell, A. Benatar, J. B. Park, and C. Bonten, *Plastics and composites welding handbook LK - https://northdakotastateuniversitylibrary.on.worldcat.org/oclc/318407015*. Munich SE - xv, 407 p. : il. ; 24 cm: Hanser, 2003.

[6] D. Grewell and A. Benatar, “Welding of Plastics: Fundamentals and New Developments,” *Int. Polym. Process.*, vol. 22, no. 1, pp. 43–60, 2007.

[7] J. Vogel, “Sealing and cutting of PLA bio-plastic,” Doctoral dissertation, Department of Mechanical Engineering, Iowa State University, Ames, IA, 2011. Accessed on: September 6, 2021. [Online]. Available: https://lib.dr.iastate.edu/etd/14131/

[8] S. Liu and I. Chang, “Optimizing the Weld Strength of Ultrasonically Welded Nylon Composites,” *Journal of Composite Materials*, vol. 36, no. 05, pp. 611-624, 2002.

[9] K. Eunseob, S. Yong-Jun, and A. Sung-Hoon, “The effects of moisture and temperature on the mechanical properties of additive manufacturing components: fused deposition modeling,” *Rapid Prototyp. J.*, vol. 22, no. 6, pp. 887–894, Jan. 2016.

[10] S. N. A. M. Halidi and J. Abdullah, “Moisture and humidity effects on the ABS used in Fused Deposition Modeling machine,” *Adv. Mater. Res.*, vol. 576, pp. 641–644, 2012.

[11] R. J. Zaldivar, T. D. Mclouth, G. L. Ferrelli, D. N. Patel, A. R. Hopkins, and D. Witkin, “Effect of initial filament moisture content on the microstructure and mechanical performance of ULTEM ® 9085 3D printed parts,” *Addit. Manuf.*, vol. 24, no. July, pp. 457–466, 2018.

[12] C. Hopmann and A. Van Aaken, “Ultrasonic welding of polyamide — influence of moisture on the process relevant material properties,” pp. 787–793, 2014.

[13] Q. Zhi, X. R. Tan, and Z. X. Liu, “Effect of Moisture on the Ultrasonic Welding of Carbon - Fiber - Reinforced Polyamide 66 Composite,” *The Welding Journal*, vol. 96, pp. 185-192, June, 2017.

[14] S. J. Christian and S. L. Billington, “Moisture diffusion and its impact on uniaxial tensile response of biobased composites,” *Compos. Part B Eng.*, vol. 43, no. 5, pp. 2303–2312, 2012.

[15] V. A. Alvarez, A. N. Fraga, and A. Vázquez, “Effects of the moisture and fiber content on the mechanical properties of biodegradable polymer-sisal fiber biocomposites,” *J. Appl. Polym. Sci.*, vol. 91, no. 6, pp. 4007–4016, 2004.

[16] N. Sombatsompop and K. Chaochanchaikul, “Effect of moisture content on mechanical properties, thermal and structural stability and extrudate texture of poly(vinyl chloride)/wood sawdust composites,” *Polym. Int.*, vol. 53, no. 9, pp. 1210–1218, 2004.

[17] H. Pan and X. S. Sun, “Effects of Moisture Content and Extrusion Parameters on Tensile Strength of Starch and Poly(Lactic Acid) Blends,” *Applied Engineering in Agriculture*, vol. 19, no. 5, pp. 573–579, 2003.
[18] E. Kim, Y. J. Shin, and S. H. Ahn, “The effects of moisture and temperature on the mechanical properties of additive manufacturing components: Fused deposition modeling,” *Rapid Prototyp. J.*, vol. 22, no. 6, pp. 887–894, 2016.
[19] I. T. Garces, S. Aslanzadeh, Y. Boluk, and C. Ayranci, “Effect of moisture on shape memory polyurethane polymers for extrusion-based additive manufacturing,” *Materials (Basel).*, vol. 12, no. 2, 2019.
[20] N. Stoehr, B. Baudrit, E. Haberstroh, M. Nase, P. Heidemeyer, and M. Bastian, “Ultrasonic welding of plasticized PLA films,” *J. Appl. Polym. Sci.*, vol. 132, no. 4, pp. 1–8, 2015.
[21] J. Vogel, D. Grewell, M. R. Kessler, D. Drummer, and M. Menacher, “Ultrasonic and Impulse Welding of Polylactic Acid Films,” *Polym. Eng. Sci.*, vol. 51, no. 6, pp. 1059–1067, 2011.
[22] Z. Kiss, T. Temesi, and T. Czigány, “Adherability and weldability of poly(lactic acid) and basalt fibre-reinforced poly(lactic acid),” *J. Adhes. Sci. Technol.*, vol. 32, no. 2, pp. 173–184, 2018.
[23] K. E. Lebron, “Interfacial healing and transport phenomena modeling of biopolymers,” M.S. thesis, Department of Agricultural and Biosystems Engineering, Iowa State University, Ames, IA, 2017. Accessed on: July 7, 2021. [Online]. Available: https://lib.dr.iastate.edu/etd/16161/
[24] X. Wang, M. Jiang, Z. Zhou, J. Gou, and D. Hui, “3D printing of polymer matrix composites: A review and prospective,” *Compos. Part B Eng.*, vol. 110, pp. 442–458, 2017.
[25] A. Dey and N. Yodo, “A systematic survey of FDM process parameter optimization and their influence on part characteristics,” *J. Manuf. Mater. Process.*, vol. 3, no. 3, 2019.
[26] J. Lunt, “Large-scale production, properties and commercial applications of poly lactic acid polymers,” *Polym. Degrad. Stab.*, vol. 59, no. 1–3, pp. 145–152, 1998.
[27] B. Tyler, D. Gullotti, A. Mangraviti, T. Utsuki, and H. Brem, “Polylactic acid (PLA) controlled delivery carriers for biomedical applications,” *Adv. Drug Deliv. Rev.*, vol. 107, pp. 163–175, 2016.
[28] J. K. Oh, “Polylactide (PLA)-based amphiphilic block copolymers: Synthesis, self-assembly, and biomedical applications,” *Soft Matter*, vol. 7, no. 11, pp. 5096–5108, 2011.
[29] A. J. R. Lasprilla, G. A. R. Martinez, B. H. Lunelli, A. L. Jardini, and R. M. Filho, “Poly-lactic acid synthesis for application in biomedical devices - A review,” *Biotechnol. Adv.*, vol. 30, no. 1, pp. 321–328, 2012.
[30] M. M. Reddy, S. Vivekanandhan, M. Misra, S. K. Bhatia, and A. K. Mohanty, “Biobased plastics and bionanocomposites: Current status and future opportunities,” *Prog. Polym. Sci.*, vol. 38, no. 10–11, pp. 1653–1689, 2013.
[31] R. M. Rasal, A. V. Janorkar, and D. E. Hirt, “Poly(lactic acid) modifications,” *Prog. Polym. Sci.*, vol. 35, no. 3, pp. 338–356, 2010.
[32] M. Gigli, M. Fabbri, N. Lotti, R. Gamberini, B. Rimini, and A. Munari, “Poly(butylene succinate)-based polyesters for biomedical applications: A review in memory of our beloved colleague and friend Dr. Lara Finelli.,” *Eur. Polym. J.*, vol. 75, pp. 431–460, 2016.

[33] K. Chrissafis, K. M. Paraskevopoulos, and D. N. Bikiaris, “Thermal degradation mechanism of poly(ethylene succinate) and poly(butylene succinate): Comparative study,” *Thermochim. Acta*, vol. 435, no. 2, pp. 142–150, 2005.
[34] R. P. Babu, K. O’Connor, and R. Seeram, “Current progress on bio-based polymers and their future trends,” *Prog. Biomater.*, vol. 2, no. 1, p. 8, 2013.
[35] S. A. Grammatikos, B. Zafari, M. C. Evernden, J. T. Mottram, and J. M. Mitchels, “Moisture uptake characteristics of a pultruded fibre reinforced polymer flat sheet subjected to hot/wet aging,” *Polym. Degrad. Stab.*, vol. 121, pp. 407–419, 2015.
[36] R. Šturm, R. Grimberg, A. Savin, and J. Grum, “Destructive and nondestructive evaluations of the effect of moisture absorption on the mechanical properties of polyester-based composites,” *Compos. Part B Eng.*, vol. 71, pp. 10–16, 2015.
[37] S. J. Christian and S. L. Billington, “Moisture diffusion and its impact on uniaxial tensile response of biobased composites,” *Compos. Part B Eng.*, vol. 43, no. 5, pp. 2303–2312, 2012.
[38] C. Carfagna, A. Apicella, and L. Nicolais, “The effect of the prepolymer composition of amino-hardened epoxy resins on the water sorption behavior and plasticization,” *J. Appl. Polym. Sci.*, vol. 27, no. 1, pp. 105–112, 1982.
[39] H. Alamri and I. M. Low, “Effect of water absorption on the mechanical properties of nano-filler reinforced epoxy nanocomposites,” *Mater. Des.*, vol. 42, pp. 214–222, 2012.
[40] W. G. Knauss and V. H. Kenner, “On the hygrothermomechanical characterization of polyvinyl acetate,” *J. Appl. Phys.*, vol. 51, no. 10, pp. 5131–5136, 1980.
[41] M. Qahtani, F. Wu, M. Misra, S. Gregori, D. F. Mielewski, and A. K. Mohanty, “Experimental Design of Sustainable 3D-Printed Poly(Lactic Acid)/Biobased Poly(Butylene Succinate) Blends via Fused Deposition Modeling,” *ACS Sustain. Chem. Eng.*, vol. 7, no. 17, pp. 14460–14470, 2019.
[42] T. Y. Qiu, M. Song, and L. G. Zhao, “Testing, characterization and modelling of mechanical behaviour of poly (lactic-acid) and poly (butylene succinate) blends,” *Mech. Adv. Mater. Mod. Process.*, vol. 2, no. 1, 2016.
[43] J. W. Park and S. S. Im, “Phase behavior and morphology in blends of poly(L-lactic acid) and poly(butylene succinate),” *J. Appl. Polym. Sci.*, vol. 86, no. 3, pp. 647–655, 2002.
[44] E. S. Yoo and S. S. Im, “Melting behavior of poly(butylene succinate) during heating scan by DSC,” *J. Polym. Sci. Part B Polym. Phys.*, vol. 37, no. 13, pp. 1357–1366, 1999.
[45] X. Wang, J. Zhou, and L. Li, “Multiple melting behavior of poly(butylene succinate),” *Eur. Polym. J.*, vol. 43, no. 8, pp. 3163–3170, 2007.
[46] K. Pölöskei, G. Csézi, S. Hajba, and T. Tábi, “Investigation of the thermoformability of various D-Lactide content poly(lactic acid) films by ball burst test,” *Polym. Eng. Sci.*, vol. 60, no. 6, pp. 1266–1277, 2020.
[47] B. A. W. Keong and R. Y. C. Hua, “A Novel Fold-Based Design Approach toward Printable Soft Robotics Using Flexible 3D Printing Materials,” *Adv. Mater. Technol.*, vol. 3, no. 2, pp. 1–12, 2018.
[48] S. N. B. and H. J. C. Amita Bhatia, Rahul K. Gupta, “Compatibility of biodegradable PLA and PBS blens for packaging application(2007).pdf,” *Rheology Journal*, vol. 19, no. 3. pp. 125–131, 2007.
[49] L. Jompang *et al.*, “Poly(lactic acid) and poly(butylene succinate) blend fibers prepared by melt spinning technique,” *Energy Procedia*, vol. 34, pp. 493–499, 2013.

[50] Y. Deng and N. L. Thomas, “Blending poly(butylene succinate) with poly(lactic acid): Ductility and phase inversion effects,” *Eur. Polym. J.*, vol. 71, pp. 534–546, 2015.
[51] Q. Ou-Yang, B. Guo, and J. Xu, “Preparation and Characterization of Poly(butylene succinate)/Polylactide Blends for Fused Deposition Modeling 3D Printing,” *ACS Omega*, vol. 3, no. 10, pp. 14309–14317, 2018.
[52] B. N. Turner and S. A. Gold, “A review of melt extrusion additive manufacturing processes: II. Materials, dimensional accuracy, and surface roughness,” *Rapid Prototyp. J.*, vol. 21, no. 3, pp. 250–261, 2015.
[53] D. Ahn, J. H. Kweon, S. Kwon, J. Song, and S. Lee, “Representation of surface roughness in fused deposition modeling,” *J. Mater. Process. Technol.*, vol. 209, no. 15–16, pp. 5593–5600, 2009.
[54] R. Homklin and N. Hongsriphan, “Mechanical and Thermal Properties of PLA/PBS Co-continuous Blends Adding Nucleating Agent,” *Energy Procedia*, vol. 34, pp. 871–879, Jan. 2013.
[55] T. Yokohara and M. Yamaguchi, “Structure and properties for biomass-based polyester blends of PLA and PBS,” *Eur. Polym. J.*, vol. 44, no. 3, pp. 677–685, Mar. 2008.
[56] S. Su, R. Kopitzky, S. Tolga, and S. Kabasci, “Polylactide (PLA) and its blends with poly(butylene succinate) (PBS): A brief review,” *Polymers (Basel).*, vol. 11, no. 7, pp. 1–21, 2019.
[57] X. Hu, T. Su, P. Li, and Z. Wang, “Blending modification of PBS/PLA and its enzymatic degradation,” *Polym. Bull. 2017 752*, vol. 75, no. 2, pp. 533–546, May 2017.
[58] T. Messin *et al.*, “Biodegradable PLA/PBS multinanolayer membrane with enhanced barrier performances,” *J. Memb. Sci.*, vol. 598, p. 117777, Mar. 2020.
[59] S. J. Zhang, Y. W. Tang, and L. H. Cheng, “Biodegradation Behavior of PLA/PBS Blends,” *Adv. Mater. Res.*, vol. 821–822, pp. 937–940, 2013.
[60] H. K. Liu, W. L. Dai, and Y. C. Lee, “Moisture effects and acoustic emission characterization on lap shear strength in ultrasonic welded carbon/nylon composites,” *J. Mater. Sci.*, vol. 35, no. 13, pp. 3389–3396, 2000.

APPENDIX. ALGORITHM FOR % POROSITY CALCULATION

Data: Image of the printed material
Result: Estimation of the porosity of the material
Apply a Gaussian Filter to blur the image
$gapPixels \leftarrow 0$;
for *each pixel in the image* **do**
  if $pixelColor \leq threshold$ **then**
    if *Three surrounding pixels are below the threshold* **then**
      $gapPixels \leftarrow gapPixels + 1$;
    end
  end
end
$porosity \leftarrow gapPixels/totalPixels$;

Algorithm 1: Pixel Count Algorithm. This algorithm blurs the image, then checks each pixel and its surroundings. If the pixel and a large enough portion of its surroundings are below the user-defined threshold, then the pixel is counted as part of a pore.